A sleep-active neuron can promote survival while sleep behavior is disturbed

Inka Busack[1], Henrik Bringmann[1]*

[1] BIOTEC, Technical University Dresden, Germany

*Corresponding author: henrik.bringmann@tu-dresden.de

Abstract

Sleep is controlled by neurons that induce behavioral quiescence and physiological restoration. It is not known, however, how sleep neurons link sleep behavior and survival. In *Caenorhabditis elegans*, the sleep-active RIS neuron induces sleep behavior and is required for survival of starvation and wounding. Sleep-active neurons such as RIS might hypothetically promote survival primarily by causing sleep behavior and associated conservation of energy. Alternatively, RIS might provide a survival benefit that does not depend on behavioral sleep. To probe these hypotheses, we tested how activity of the sleep-active RIS neuron in *Caenorhabditis elegans* controls sleep behavior and survival during larval starvation. To manipulate the activity of RIS, we expressed constitutively active potassium channel (*twk-18gf* and *egl-23gf*) or sodium channel (*unc-58gf*) mutant alleles in this neuron. Low levels of *unc-58gf* expression in RIS increased RIS calcium transients and sleep. High levels of *unc-58gf* expression in RIS elevated baseline calcium activity and inhibited calcium activation transients, thus locking RIS activity at a high but constant level. This manipulation caused a nearly complete loss of sleep behavior but increased survival. Long-term optogenetic activation also caused constantly elevated RIS activity and a small trend towards increased survival. Disturbing sleep by lethal blue-light stimulation also overactivated RIS, which again increased survival. FLP-11 neuropeptides were important for both, induction of sleep behavior and starvation survival, suggesting that FLP-11 might have divergent roles downstream of RIS. These results indicate that promotion of sleep behavior and survival are separable functions of RIS. These two functions may normally be coupled but can be uncoupled during conditions of strong RIS activation or when sleep behavior is impaired. Through this uncoupling, RIS can provide survival benefits under conditions when behavioral sleep is disturbed. Promoting survival in the face of impaired sleep might be a general function of sleep neurons.

Author Summary

The sleep neuron RIS in *Caenorhabditis elegans* is required to induce sleep behavior and to promote survival upon stress. Here we show that RIS can provide survival benefits even when sleep is disturbed.

Introduction

Sleep is defined by behavioral inactivity and reduced responsiveness [1]. It is a physiological state that conserves and allocates energy, promotes restorative processes, and is important for brain and cognitive functions [2-4]. Sleep disorders and deviations from the normal sleep amount are widespread in modern societies and pose an unresolved medical and economical problem [5-7].

Sleep is found in most animals ranging from cnidarians to humans. Central to the induction of sleep in all species are so-called sleep-active neurons that activate to inhibit wakefulness behavioral circuits and thus cause sleep behavior [8, 9]. *C. elegans* has a small and invariant nervous system and sleep is controlled by relatively few neurons. RIS is a GABAergic and peptidergic interneuron that activates during sleep, and its ablation virtually abolishes sleep behavior during molting of developing larvae, in arrested larvae, and in adults following cellular stress [10-21]. Optogenetic manipulations showed that acute activation of RIS inhibits wakefulness activity such as feeding and locomotion [10, 15], whereas inactivation of RIS inhibits sleep [12, 18, 22, 23]. RIS is important for survival during starvation and after wounding [12, 18, 24]. This neuron counteracts aging phenotype progression during starvation-induced arrest [12]. It supports the protective transcriptional response that underlies the arrest, and promotes the activity of the FOXO transcription factor DAF-16, which is required for survival [24-26]. Thus, RIS is a sleep-active neuron that is crucial for *C. elegans* sleep and stress survival.

Little is known about how sleep-active neurons such as RIS link sleep behavior and survival. Different hypotheses are conceivable. For example, sleep-active neurons might promote survival by reducing behavioral activities during sleep, thus conserving and allocating energy or optimizing behavior [27, 28]. The close association of sleep and physiological benefits has suggested a causal relationship. For example, memory and information processing are thought to be improved in the human brain during sleep when information inputs are blocked [29, 30], and energy is conserved by reduced behavioral activity [28]. A less explored additional hypothesis is that sleep-active neurons provide benefits during sleep, but independently of sleep behavior. According to this hypothesis,

sleep-active neurons have two parallel functions. The first is to induce sleep behavior, and the second is to promote survival. This hypothesis implies that physiological benefits of sleep-active neuron functions can be exerted also when sleep behavior is impaired.

In order to find out how RIS links sleep and survival, we manipulated RIS activity through transgenic expression of ion channel mutants in RIS. By strongly expressing *unc-58gf* in RIS, we achieved an overall increase of RIS activity that was caused by constantly elevated baseline calcium activity in RIS. RIS appeared to be locked at this higher activity level, as it was not able to activate further upon stimulation. Survival was increased in this strain, but sleep behavior was almost completely lacking. The sleep loss phenotype included a lack of dampening of the activity of interneurons, sensory neurons and muscles that is typical for normal sleep. Thus, strong expression of RIS led to an apparent uncoupling of sleep behavior and survival. Long-term optogenetic activation also generated constantly increased calcium activity and a small trend towards increased survival. Stimulation with blue light disturbed sleep and increased RIS activation, which in turn extended survival. Finally, we find that RIS promotes sleep behavior and promotes survival through FLP-11 neuropeptides.

RIS hence appears to be able to promote survival independently of sleep behavior, indicating that promotion of sleep behavior and survival are separable functions of RIS that are normally coupled during sleep but that can be uncoupled. Uncoupling appears to occur during conditions of stimulation that disturb sleep and increase RIS activity. This suggests that an important function of RIS overactivation is to promote survival not only during normal sleep, but also and in particular when sleep behavior is disturbed. Sleep-active neurons might generally function to promote survival both during normal sleep and even more so when sleep behavior is disturbed.

Results

Generation of a strain set for controlling RIS activity

100

101 We set out to control RIS activity to study sleep and survival during L1 arrest. For this
102 study, we generated strains that express constitutively active ion channels with different
103 ion permeability and expression levels in RIS. To constitutively inactivate RIS, we
104 expressed potassium channels that carry mutations that cause potassium leak currents using
105 the *flp-11* promotor that is strong and highly specific for RIS [11, 17, 31]. We used two
106 different *egl-23* channel mutations to achieve different strengths of inactivation of RIS
107 (*RIS::egl-23gf(weak)* expresses *egl-23(L229N)* in RIS, *RIS::egl-23gf(strong)* expresses
108 *egl-23(A383V)* in RIS) [32]. To create a strong tool for RIS inhibition, we expressed a *twk-*
109 *18* mutant allele that is known to cause a very strong potassium current (*RIS::twk-18gf*
110 expresses *twk-18(e1913)* in RIS) [33]. In all three strains, the channel genes were knocked
111 into the endogenous *flp-11* locus behind the *flp-11* gene to generate operons that express
112 both *flp-11* and the mutant ion channel. All fusion proteins localized to the cell membrane
113 of RIS (Fig 1A-D).

114

115 To constitutively over activate RIS, we used an unusual K2P channel mutant that is
116 permeable to sodium [32] (Thomas Boulin, personal communication). We expressed the
117 ion channel mutant in RIS (*unc-58(L428F),* Fig S1A) tagged with mKate2 at either a lower
118 or a higher level in RIS. The different expression levels were achieved by generating two
119 different expression loci for the channel in the genome. To achieve a strong expression of
120 the *unc-58(L428F)* channel (*RIS::unc-58gf(strong)*), we turned the endogenous *flp-11*
121 locus into an operon as above. To achieve a weaker expression of the channel (*RIS::unc-*
122 *58gf(weak)*), we expressed mKate2-tagged *unc-58(L428F)* from a single-copy knock-in
123 locus on chromosome III [34], which contained only a minimal *flp-11* promoter and 3'
124 UTR [11] (Fig 1 E-H). Fluorescent imaging after two days of L1 arrest showed that the
125 stronger strain expressed at about double the level of the weaker strain and in both
126 transgenes, the channel was expressed prominently in RIS and was targeted to the cell
127 membrane (Fig 1E-H, S1). Even after 21 days of arrest, mKate2-tagged *unc-58(L428F)*
128 expression could be detected in the strong strain indicating that the sodium channel mutant
129 is properly folded and targeted to the plasma membrane across the entire arrest (FigS1E).

130

131

132 ***RIS::unc-58gf(strong)* promotes survival of L1 arrest**

133

134 Previous studies have shown that RIS is required for survival during larval arrest and
135 following wounding of the adult [12, 18, 35]. RIS activity controls the gene expression
136 changes that underly the physiological adaptation to starvation [24]. *RIS::unc-58gf(strong)*
137 and *RIS::twk-18gf* displayed opposing gene expression changes compared with the wild
138 type. *RIS::twk-18gf* is more similar to *aptf-1(-)*, which causes loss of RIS function [10, 24].
139 To identify additional genes whose expression depend on RIS activity, we directly
140 compared the gene expression profiles of *RIS::unc-58gf(strong)* and *RIS::twk-18gf* during
141 L1. This analysis identified 4676 differentially expressed genes including 1910 novel genes
142 that were not previously reported to be controlled by RIS (Fig 2A, Table S5). This
143 comparison confirms the notion that activation and inactivation of RIS have opposing
144 effects on gene expression [24]. These data support the idea that the expression of *twk-18gf*
145 and *unc-58gf* in RIS cause RIS inactivation and RIS activation gene expression phenotypes,
146 respectively [24].

147

148 To get an understanding of the role of RIS activation on survival, we investigated how the
149 different RIS-expressed ion channels affect survival in arrested L1 larval worms. For this
150 experiment, we kept arrested L1 larvae as liquid culture, as this allowed for a higher
151 number of animals to be processed. We regularly took a sample of the larvae from the
152 liquid culture and measured two different readouts. We first measured starvation survival
153 by scoring the fraction of animals that had survived and secondly, we scored the ability of
154 starved animals to recover and develop to the adult stage after refeeding [12, 23, 24, 36].
155 *RIS::twk-18gf* larvae showed strongly reduced starvation survival by about half compared
156 to the wild type. *egl-23(strong)* resulted in a more moderate yet significant starvation
157 survival reduction of approximately 21%. Weak inactivation by *egl-23(weak)* or
158 overactivation by *unc-58gf(weak)* of RIS activity did not significantly change starvation
159 survival. Strong RIS overactivation by *unc-58gf(strong)* had an increased starvation
160 survival of around 19% compared to wild type (Fig 2B). These results are in accordance
161 with previous reports and the expected changes caused by the ion channel transgenes [12,

24, 32, 33]. The recovery upon refeeding matched the survival curves (Fig 2C). To test whether this survival-extending effect was caused by *unc-58gf* expression in RIS, we measured survival of *RIS::unc-58gf(strong)* in an *aptf-1(-)* background, in which expression of *unc-58gf* in RIS is abolished (Fig S1G). In the combined *RIS::unc-58gf(strong); aptf-1(-)* strain starvation survival was extremely shortened compared with wild type (Fig S2) and was similar to *aptf-1(-)* [12] or *RIS::twk-18gf* (Fig 2B), indicating that the starvation survival extension indeed stemmed from *unc-58gf* expression in RIS.

Ion channel mutant expression in RIS controls baseline RIS activity

How are RIS activity, sleep behavior and survival linked? To shed light on this question, we imaged RIS calcium activity in these mutants. [10]. We used microfluidic chambers to keep and image the larvae. This method allowed for a quantification of RIS baseline activity, RIS calcium activation transients, and sleep behavior [37, 38]. We were able to measure RIS activity for the first 12 days of starvation, and found that the effects of the channel transgenes were consistent across the entire time of starvation that we analyzed (Fig 3A for two-day starvation, 3B for all time points). We first analyzed the baseline activity of RIS in the absence of calcium transients. The mean RIS baseline calcium activity levels were reduced by the strongly inactivating transgenes *twk-18gf* and *egl-23gf(strong)*. Baseline activity levels were modestly increased by *unc-58gf(weak)* and strongly increased by *unc-58gf(strong)*. The magnitude of the baseline calcium signal alterations of the different transgenes were thus in accordance with the expression levels and the expected strengths of the leak currents (Fig 1F). These data demonstrate that transgenic *unc-58gf* can be used as a tool for increasing calcium activity in a neuron that does not normally express *unc-58* [17, 31, 32]. We used these tools to create a set of strains that allows for probing associations of baseline activity levels and survival as well as sleep.

***RIS::unc-58gf(strong)* inhibits sleep behavior during L1 arrest**

193 We next quantified motion quiescence as a readout for sleep and tracked mobility behavior
194 during L1 arrest inside microfluidic chambers. We used GCaMP fluorescence to quantify
195 RIS activation transients across the entire measurement [10]. Consistent with previous
196 reports [10, 12, 20], wild-type RIS showed activation transients over a constant baseline,
197 and calcium transients were accompanied by phases of behavioral quiescence (Fig 4A-G).
198 Calcium transients were completely abolished in both the strongest deactivation strains
199 (Fig 4A, B) as well as in the strong activation strain (4F). In the mild deactivation strain
200 calcium transients were still visible and correlated with behavioral quiescence, but were
201 decreased in magnitude (Fig 4C/G, S3A). In *RIS::unc-58gf(weak)*, RIS calcium transient
202 activity and bouts of behavioral activity were increased (Fig 4E). These results suggest that
203 RIS activation transients are required for sleep induction and that strong inactivation
204 prevents these transients. Mobility quiescence decreased with inactivation and was
205 increased with modest activation as expected. We anticipated that the elevated RIS calcium
206 baseline of *RIS::unc-58gf(strong)* might be associated with a further increase in sleep
207 behavior compared with the weak activation. Mobility quiescence was, however,
208 completely abolished by strong RIS activation in most of the animals (Fig 4H). These
209 findings were additionally confirmed for a longer period of starvation up to day 12 (Fig
210 4I). The loss of quiescence of the strong RIS activation strain was similar to, but not as
211 strong as in *aptf-1(-)* (Fig S2B). The sleep amounts for each strain are consistent for several
212 days in L1 arrest (Fig 4I). In summary, baseline RIS activity correlates with behavioral
213 quiescence over a wide range of conditions, except for the *RIS::unc-58gf(strong)*
214 transgene, which appears to cause a lack of RIS calcium transients and sleep behavior.
215
216
217 ***RIS::unc-58gf* impairs sleep behavior during larval development and following**
218 **cellular stress in the adult**
219
220 *C. elegans* sleeps during various stages and conditions. Previous studies showed that
221 cellular stress increases adult sleep [17, 39-42]. During development, sleep is coupled to
222 the molting cycle and occurs during a period called lethargus, which coincides with
223 formation of a new cuticle [10, 43, 44]. To test whether constant RIS baseline activation is

224 also associated with a loss of behavioral quiescence during stress-induced sleep and during
225 lethargus sleep, we tested whether *RIS::unc-58gf* affects sleep behavior during L1
226 development as well as following heat stress. For testing for stress-induced sleep, we kept
227 young adult worms inside microfluidic devices and first measured baseline behavioral
228 activity at 22°C, and then exposed the animals to heat stress at 37°C for 20 minutes. We
229 then followed the behavior again after the end of the heat shock [17]. The wild type
230 immobilized during the heat shock and displayed an increase in behavioral quiescence
231 following the heat shock. The quiescence response was attenuated in all strains in which
232 RIS was manipulated. Both *unc-58gf* expressing strains showed decreased behavioral
233 quiescence. Thus, a reduction of behavioral sleep can also be caused by *RIS::unc-*
234 *58gf(weak)* (Fig 5A-G).
235
236 To test for sleep that occurs during development, we quantified behavioral quiescence of
237 *RIS::unc-58gf(strong)* during lethargus in fed L1 larvae. Behavioral quiescence of
238 *RIS::unc-58gf(strong)* was significantly reduced compared with the wild type. The loss of
239 sleep behavior in lethargus was, however, not as strong as during L1 arrest or following
240 stress-induced sleep (Fig 5H). Hence, in all the stages and conditions that we tested, sleep
241 behavior was reduced by *RIS::unc-58gf(strong)*.
242
243 We also tested whether the lack of sleep behavior in *RIS::unc-58gf(strong)* during L1 arrest
244 causes a compensatory increase in sleep when the animals resume development. For this
245 experiment, we starved larvae for 12 days and then provided them with food, which
246 allowed for a resumption of development. We then imaged sleep behavior during L1
247 lethargus in these recovered worms. There was no increase of sleep behavior in recovered
248 *RIS::unc-58gf(strong)* larvae compared with wild type (Fig S4). Thus there was no
249 indication for rebound sleep occurring at the subsequent lethargus stage in *RIS::unc-*
250 *58gf(strong)*.
251
252
253 ***RIS::unc-58gf(strong)* impairs the dampening of wake-active neuronal circuits**
254 **during L1 arrest**

255

256 *RIS::unc-58gf(strong)* caused strongly reduced sleep behavior, but the nature of the
257 residual sleep behavior in this mutant was unclear. Did the residual sleep behavior present
258 a generally weakened sleep state or a compensatory deep sleep state? To answer this
259 question, we characterized neuronal activity during in *RIS::unc-58gf(strong)* mutants. For
260 this set of experiments, we imaged larvae in microfluidic chambers and imaged neuronal
261 activity with GCaMP during L1 starvation-induced arrest.

262

263 *C. elegans* sleep is characterized as a state of globally reduced nervous system activity [12,
264 13, 20]. We measured the overall neuronal activity by utilizing a strain that expresses
265 GCaMP6s in all neurons [45]. We measured both motion behavior and overall neuronal
266 activity by extracting the calcium activity signal of all neurons as one combined signal [12,
267 22]. Consistent with previous reports, periods of behavioral quiescence were accompanied
268 by strongly reduced global neuronal activity (Fig 6A, B, S5) [12, 13, 20, 22]. We extracted
269 phases of neuronal inactivity as well as phases of behavioral inactivity from the data set.
270 In all strains, neuronal inactivity directly correlated with immobility, suggesting that
271 behavioral quiescence and neuronal quiescence are correlated in all strains irrespective of
272 the level of RIS baseline activity (Fig 6C). Thus, both behavioral inactivity and brain
273 inactivity can serve as equivalent readouts for detecting sleep in this system. Strong RIS
274 inactivation led to an increased mean overall neuronal activity of 50.7% compared to wild
275 type. Intermediate strength of inactivation did not affect mean overall neuronal activity.
276 *RIS::unc-58gf(strong)* caused a significant increase of mean overall neuronal activity of
277 35.7% (Fig 6D). These results support the notion that *RIS::unc-58gf(strong)* worms are in
278 a state of wakefulness for most of the time and lack phases of strong nervous system
279 activity dampening.

280

281

282 To characterize the effects of *RIS::unc-58gf(strong)* at the level of specific individual
283 neurons, we imaged activity of the RIM neurons, which are second layer interneurons that
284 integrate information from sensory and internal states to control motion behaviors [46, 47].
285 Again, we used GCaMP imaging in microfluidic chambers to correlate neuronal and

286 behavioral activity. RIM showed activation transients during phases of behavioral activity.
287 During phases of behavioral quiescence, RIM activity was strongly reduced and activation
288 transients were lacking (Fig 6E, F, S6). Similar to the pan-neuronal measurements, the time
289 fraction during which RIM was inactive correlated with phases of motion quiescence (Fig
290 6G). Consistent with the pan-neuronal imaging data, *RIS::unc-58gf(strong)* lacked phases
291 of RIM inactivity (Fig 6H).
292
293 An increased arousal threshold and attenuated sensory information processing are key
294 characteristics of sleep [1, 48]. In *C. elegans*, sensory information processing is inhibited
295 during sleep in developing larvae and the activity of sensory neurons is reduced [49-51].
296 For example, the mechanosensory neurons ALM and PLM display dampened activation
297 transients during sleep in developing L1 larvae [49, 50]. We measured PLM activity in
298 wild-type, *RIS::unc-58gf(strong)* and *RIS::twk-18gf* larvae. In wild-type animals, PLM
299 showed activation transients only during phases of wakefulness, whereas PLM appeared
300 to be rather inactive during sleep. In both *RIS::unc-58gf(strong)* and *RIS::twk-18gf*
301 mutants, PLM showed activation transients almost continuously throughout the time, with
302 only small episodes where PLM seemed to be not active (Fig 7). Thus, extended periods
303 of PLM neuron inactivity were absent in both *RIS::unc-58gf(strong)* and *RIS::twk-18gf*
304 mutants. Thus, *RIS::unc-58gf(strong)* inhibits the dampening of neuronal activity that is
305 associated with wakefulness behavior and thus lacks the neuronal signature of deep sleep.
306
307
308 ***RIS::unc-58gf(strong)* promotes muscle activity**
309
310 An absence of voluntary movement, reduced muscle contraction and a relaxed body
311 posture are hallmarks of sleep across species including *C. elegans* [44, 52-54]. If *RIS::unc-*
312 *58gf(strong)* lacks deep sleep bouts then this should be reflected by the absence of extended
313 periods of movement quiescence that coincide with reduced muscle activity. During
314 wakefulness, *C. elegans* shows locomotion behavior and feeds by contractions of the
315 pharynx muscle [55, 56]. Locomotion and pharyngeal pumping stops during sleep and the
316 animals assume a relaxed body posture [10, 44, 52, 54]. Underlying these effects, RIS

317 inhibits both locomotion and pharyngeal pumping [10, 12, 15, 57, 58]. To test the
318 hypothesis that *RIS::unc-58gf(strong)* lacks long phases of muscle relaxation that are
319 typical for sleep, we first imaged arrested larvae inside microfluidic chambers and
320 quantified more precisely movement activity of the body and the pharynx.
321
322 To quantify mobility behavior of the head and tail regions, we tracked the positions of
323 neurons that are located in these body parts. To calculate movement speed of the head, we
324 tracked the position of the RIM neurons. For tracking the tail we used the position of the
325 PLM neurons [59]. The tracking data revealed that in *RIS::twk-18gf*, both head and tail
326 movement was similar to the wild type during wakefulness. During the few quiescence
327 phases of *RIS::twk-18gf*, movement speed was reduced less than in the wild type, indicating
328 that the quiescence phases that remain in *RIS::twk-18gf* are less pronounces compared with
329 the wild type. In *RIS::unc-58gf(strong)*, head movement was decreased compared to wild-
330 type worms, whereas there was no difference in tail movement (Fig 8A-B). *RIS::unc-*
331 *58gf(strong)* worms were uncoordinated and the body was more curved (Fig S7, Movies
332 S7 and S8), which might explain the difference of head and tail movement speeds. In the
333 few locomotion quiescence phases of *RIS::unc-58gf(strong)*, there appeared to be less of a
334 reduction of movement speed.
335
336 We next imaged our transgenic strains in the arrested first larval stage for 1 min with a
337 framerate of 10Hz and manually scored pumping rate. This analysis revealed no significant
338 difference in pharyngeal contraction rates for all strains compared to wild type (Fig S8).
339
340 To test how *RIS::unc-58gf(strong)* and *RIS::twk-18gf* affect muscle activity, we measured
341 and quantified muscle GCaMP [52]. In the wild type, muscle calcium activity was high
342 during wakefulness, and strongly reduced during sleep. In *RIS::twk-18gf*, muscle calcium
343 was almost constantly elevated and resembled the activity levels of the wild type. *RIS::unc-*
344 *58gf(strong)* worms showed a general increase in muscle calcium activity (Fig 8C-F). The
345 increased muscle activity is consistent with and might contribute to the slightly
346 uncoordinated movement of this mutant. Phases of behavioral and muscle activity

347 dampening occurred less often, and if they occurred, then these dampened states appeared
348 to be less deep. (Fig 8G, H).
349
350
351 **In *RIS::unc-58gf(strong)*, RIS calcium activity cannot be easily elevated further by**
352 **optogenetic stimulation**
353
354 Calcium imaging suggested that the RIS baseline in *RIS::unc-58gf(strong)* is substantially
355 elevated and that calcium transients are lacking. We aimed to better understand the nature
356 of these physiological changes in RIS that are caused by expression of *RIS::unc-*
357 *58gf(strong)*. Based on the known characteristics of the *unc-58gf* mutant channel, the
358 expression of *unc-58gf* might plausibly cause a constant depolarization of the membrane
359 of RIS [32]. Depolarization in turn should lead to the activation of voltage-gated calcium
360 channels, and RIS expresses the voltage-gated calcium channels *egl-19* and *unc-2* [31].
361 The conductivity of voltage-gated calcium channels is increased by depolarization with an
362 optimum in the depolarized range. Further depolarization causes inhibition and long-term
363 stimulation reduces conductivity by desensitization [60-65]. RIS depolarization in
364 *RIS::unc-58gf(strong)* could thus perhaps be increased to allow for elevated RIS baseline
365 calcium activity, but might also inhibit further activation of calcium channel activity. We
366 tested the ability of RIS to activate by optogenetically stimulating RIS in *RIS::unc-*
367 *58gf(strong)* inside microfluidic chambers and monitored the calcium activity of this
368 neuron as well as the motion behavior of the larvae. For this experiment, we used the red-
369 shifted channelrhodopsin variant ReaChR in combination with GCaMP3 [12, 22, 57]. In
370 the wild type, optogenetic activation caused a strong increase in intracellular calcium and
371 a strong induction of motion quiescence, which is consistent with previous results [12, 15,
372 22, 57]. By contrast, optogenetic activation of RIS in *RIS::unc-58gf(strong)* did not
373 increase RIS activity further and did not induce behavioral quiescence (Fig 9A-B). This
374 result is consistent with the view that *RIS::unc-58gf(strong)* causes a heightened level of
375 RIS activity that cannot be easily increased further with optogenetic activation. Hence, in
376 *RIS::unc-58gf(strong)*, RIS appears to be locked in a state of heightened activity while
377 further activation is inhibited.

378
379
380 **Long-term optogenetic activation of RIS increases RIS baseline activity and inhibits**
381 **activation transients**
382
383 *RIS::unc-58gf(strong)* appears to cause increased RIS activity that cannot easily be
384 increased further. This could hypothetically be explained by a high level of depolarization
385 in *RIS::unc-58gf(strong)* that causes both RIS baseline elevation as well as inhibition of
386 RIS calcium transients. To test the idea that constant depolarization elevates baseline RIS
387 activity while inhibiting activation transients, we used long-term optogenetic activation.
388 We used again ReaChR to depolarize the membrane and followed the activity of RIS.
389 Optogenetic tools like ReaChR typically display a brief photocurrent peak activity within
390 the first second of light exposure and then plateau at a lower photocurrent level for an
391 extended period of time [66]. We previously used ReaChR to establish long-term
392 optogenetic manipulations in *C. elegans* [23]. To test for the activation of RIS during
393 prolonged optogenetic activation, we activated ReaChR in RIS with orange light for 11h
394 and followed the activity of RIS using GCaMP and measured mobility of the larvae that
395 were kept inside microfluidic chambers. During the first hour of optogenetic stimulation
396 of RIS, there was a strong increase of calcium activity as well as of behavioral quiescence
397 (Fig 10A-C). After this first peak period, the ongoing optogenetic stimulation led to lower
398 but more constant increase of RIS baseline activation (which was, however, weaker than
399 the activation observed in *RIS::unc-58gf(strong)* average calcium baseline activity increase
400 in *RIS::unc-58gf(strong)* compared with wild type was 1.55, and average calcium activity
401 baseline increase from 2-11h of activation in *RIS::ReaChR* compared with wild type was
402 1.25) (Fig 10D, E). Long-term optogenetic activation caused reduced calcium transients,
403 and the residual calcium transients did not correlate with phases of immobility. This
404 indicates that long-term optogenetic activation has an inhibitory effect on RIS calcium
405 transients (Fig 10F). The optogenetic long-term RIS activation did not cause a measurable
406 decrease in behavioral quiescence (Fig 10C). Thus, long-term optogenetic stimulation
407 leads to a constantly increased RIS baseline activity and an inhibition of RIS calcium
408 transients that is similar to, but weaker than, the activation observed in *RIS::unc-*

409 *58gf(strong)*. This difference in effect strength might be explained by the difference in ion
410 conductivity of these channels [32, 66]. These data indicate that long-term optogenetic
411 stimulation can lead to a constant increase in baseline RIS calcium activity at a level that
412 is above the baseline activity without optogenetic stimulation, yet lower than the maximum
413 possible optogenetic RIS activation peak intensity. These optogenetic data are consistent
414 with the idea that increased depolarization of RIS leads to a constant elevation of baseline
415 calcium activity and impairs calcium transients.
416
417
418 **Long-term optogenetic activation of RIS causes a small increase in survival**
419
420 Our data using *RIS::unc-58gf(strong)* indicated that extended survival of L1 arrest is
421 associated with increased overall RIS activity. To confirm this result with an independent
422 approach, we used *RIS::ReaChR* for long-term activation of RIS using the OptoGenBox
423 system [23]. We kept L1 larvae inside microchambers and constantly stimulated the entire
424 chambers with orange light. The optogenetic stimulation was only paused briefly once
425 every day to monitor the survival of the larvae. The stimulation protocol was applied until
426 all larvae had died. The functionality of ReaChR in *C. elegans* requires the addition of all-
427 trans retinal (ATR). Addition of ATR shortened the survival (Fig 10G). We hence
428 compared the survival of N2 exposed to ATR to worms expressing ReaChR that were also
429 exposed to ATR. By this comparison, optogenetic long-term RIS activation caused a small
430 trend for increased survival that was statistically significant according to Fisher's Exact
431 Test but not significant according to the Logrank test (p=0.02 Fisher's Exact Test, p=0.09
432 Logrank, Fig 10G). While this result borders statistical significance, it is consistent with
433 the view that activation of RIS promotes survival. The small effect size is consistent with
434 the small RIS activity increase caused by extended optogenetic stimulation. Thus, this
435 experiment supports the view that RIS activation promotes survival of L1 arrest.
436
437
438 **Lethal blue-light stimulation activates RIS, and RIS supports survival of lethal blue**
439 **light**

440

441 Disturbing sleep by sensory stimulation leads to arousal that forces wakefulness and
442 prevents the dampening of underlying neuronal circuits [12, 20, 22, 44, 67, 68]. Sleep
443 disturbance or deprivation can cause increased RIS activation [22, 24, 69]. The high level
444 of RIS activity in turn could be protective under such conditions and promote survival [24].
445 Thus, *RIS::unc-58gf(strong)* might cause a state that is similar to a state caused by
446 prolonged sleep deprivation or disturbed sleep. In both, disturbed sleep and *RIS::unc-*
447 *58gf(strong)*, the activity of wakefulness circuits is not dampened yet coincides with
448 elevated RIS activity.

449

450 To further illustrate the idea that sensory stimulation activates RIS while impairing sleep,
451 we stimulated worms with a lethal intensity of blue light. We used arrested L1 larvae after
452 48h in the absence of food, a condition during which the animals normally show regular
453 RIS activation transients and sleeping behavior [12]. We kept L1 larvae in microchambers
454 and repeatedly applied pulses of blue light while monitoring RIS activity and motion
455 behavior. For comparison, we used control animals that were exposed to shorter pulses of
456 blue light of only one tenth the length, thus still allowing for calcium imaging. Control
457 larvae displayed sleeping behavior detected by motion quiescence and RIS calcium activity
458 during about a quarter of the time (Fig 11A, B). Strong blue-light stimulation caused an
459 increase in RIS calcium activity compared with control animals (after 1h of strong blue-
460 light stimulation, the activity of RIS was approximately 5.6-fold higher compared with
461 worms that were stimulated with a lower dose). Many of the calcium transients were very
462 short, however, and did not coincide with increased motion quiescence (Fig 11B-C).
463 Hence, the stronger blue-light stimulus increased RIS activity but apparently did not
464 increase sleep behavior.

465

466 To probe for the role of RIS in survival of lethal blue-light stimulation, we compared wild-
467 type and *RIS::twk-18gf* animals, in which RIS activated less under blue-light stimulation
468 (Fig 11C). We scored the time point at which the animals became terminally immobile,
469 which presents an established proxy to score for death [70]. Control animals with
470 functional RIS died around 7-8h after strong blue-light stimulus onset. RIS-impaired

471 animals already died at around 6h after stimulus onset. The presence of functional RIS
472 hence extended survival by 15% (Fig 11D).
473
474 Thus, stimulation by a lethal blue-light stimulus can increase RIS calcium activity without
475 increasing RIS-dependent sleep behavior. While all animals were eventually killed by the
476 blue-light stimulus, RIS activity slightly extended survival. The blue-light experiment thus
477 supports the idea that RIS is a protective neuron that activates upon stressful stimulation.
478 As in *RIS::ReaChR* and during long-term optogenetic stimulation of RIS, increased RIS
479 activity was not associated with increased sleep behavior.
480
481
482 ***flp-11* is a key neuropeptide gene required for quiescence behavior in L1 arrest**
483
484 What are the key transmitters that RIS uses to control sleep during L1 arrest? GABA is
485 expressed in RIS but has not been shown to play a substantial role in promoting sleep [10,
486 15]. FLP-11 is a group of neuropeptides of RIS that present the major transmitters of RIS
487 required for sleep induction during development [11]. Expression from the *flp-11* promoter
488 depends on neuronal activity levels [71], and is increased in *RIS::unc-58gf(strong)* (Fig
489 S3B), suggesting that FLP-11 might also be a major transmitter for sleep induction during
490 L1 arrest. To directly test the role of FLP-11 in quiescence during L1 arrest, we measured
491 the effects of *flp-11* deletion (*flp-11(-)*) using microfluidic chamber imaging [11]. *flp-11(-*
492 *)* strongly reduced quiescence behavior (Fig 12A). *RIS::unc-58gf(strong)* still displayed a
493 small fraction of quiescence behavior during L1 arrest. To test whether this residual
494 quiescence was caused by *flp-11*, we deleted the entire *flp-11* gene in the *RIS::unc-*
495 *58gf(strong)* operon locus (Fig S9A) and quantified quiescence behavior. The sleep loss of
496 *RIS::unc-58gf(strong)* was reduced further by *flp-11(-),* suggesting that the residual
497 quiescence behavior in *RIS::unc-58gf* indeed depends on *flp-11* (Fig 12A).
498
499
500 **FLP-11 neuropeptides support survival**
501

502 What is the key transmitter of RIS that promotes survival? RIS is GABAergic, but GABA
503 has been suggested to be a negative regulator of lifespan [72]. We showed above that *flp-*
504 *11* is required for most of the immobility during L1 arrest sleep. We hence tested whether
505 FLP-11 neuropeptides are also required for survival. Deletion of *flp-11* reduced survival
506 by 24.7%, suggesting that *flp-11* contributes to survival (Fig 12B). To test whether *flp-11*
507 is required for increased survival caused by *RIS::unc-58gf(strong)*, we measured survival
508 in the *RIS::unc-58gf(strong), flp-11(-)* strain. *flp-11(-)* suppressed almost the entire
509 survival extension caused by *RIS::unc-58gf(strong)* (Fig 12B). Similarly, the recovery
510 upon feeding was suppressed by *flp-11(-)* in *RIS::unc-58gf(strong)* (Fig S9B). Together,
511 these experiments indicate that *flp-11* plays an important role in survival and recovery of
512 L1 arrest both in the wild type and in *RIS::unc-58gf(strong)*.
513
514 These results suggest that *flp-11* plays two roles, one role is to promote sleep and the other
515 is to promote survival. Deletion of *flp-11* blunts survival less than strong RIS inactivation,
516 indicating that additional neurosecretory factors might also contribute to survival. As RIS
517 expresses multiple neuropeptides and also GABA [11, 15, 17], it may use multiple
518 transmitters to control sleep behavior and survival. In summary these data suggest that
519 FLP-11 neuropeptides are the major transmitters released by RIS to promote both sleep as
520 well as survival during L1 arrest.
521
522
523 **Discussion**
524
525 Tools to manipulate neuronal activity are instrumental for studying neuronal circuits and
526 physiology. Here we establish the constitutively active sodium channel gene *unc-58gf* as a
527 tool for activation of a neuron that normally does not express *unc-58* [31, 32]. Modest
528 expression of *unc-58gf* in RIS during L1 arrest caused an increased baseline activity of RIS
529 and increased the probability of RIS to experience calcium activation transients. It thus
530 appears that *unc-58gf* can activate RIS when expressed at lower level. Strong expression
531 of *unc-58gf* in RIS caused constant high levels of baseline RIS activity yet prevented
532 further activation transients. When expressed highly, *unc-58gf* thus locks RIS activity at a

533 level that is higher than the normal baseline and at the same time also inhibits RIS calcium
534 transients. Thus, *unc-58gf* can be used as a tool to create different and complex patterns of
535 neuronal activity, but the level of expression is crucial to achieve different effects. Together
536 with constitutively active potassium ion channels that cause various levels of inhibition,
537 activity of a neuron can be modulated from strong inhibition to constant elevation of
538 baseline activity.
539
540 RIS inhibits wakefulness neurons to cause sleep behavior and it promotes survival under
541 stressful conditions such as larval starvation or wounding [10, 12, 18, 24, 35]. A
542 parsimonious explanation linking these two observations would be that sleep promotes
543 survival, for example through energy conservation or behavioral optimization [27]. Energy
544 conservation and behavioral optimization certainly are important functions of sleep
545 behavior [28]. In addition, sleep neurons could promote physiological benefits by
546 mechanisms that do not necessarily depend on sleep behavior.
547
548 How can the manipulation of neuronal activity be employed to solve how neurons control
549 behavioral and physiological function? Here we used transgenic expression of ion channel
550 mutants in RIS to shed light on the relationship between RIS activity, sleep behavior and
551 survival. *RIS::unc-58gf(strong)* promoted survival, but also inhibited sleep behavior. Thus,
552 *RIS::unc-58gf(strong)* allowed for an uncoupling of sleep behavior and survival functions
553 of RIS. Our data thus suggest that the sleep-active RIS neuron can promote survival
554 independently of sleep.
555
556 What are hypothetical mechanisms that allow for the uncoupling of sleep behavior and
557 survival benefits of RIS? The loss of sleep behavior in *RIS::unc-58gf(strong)* could
558 hypothetically be explained by the absence of calcium transients in RIS. This could, for
559 example, be caused by desensitization of wakefulness circuits that are downstream of RIS.
560 According to this hypothesis, wakefulness circuits would decrease their activity with
561 increasing RIS activity, and would start getting more active again only after a period of
562 stagnating or decreasing RIS activity. Both, the induction of sleep behavior and the
563 promotion of survival by RIS depend on FLP-11 neuropeptides, which are thought to be

564 released upon RIS activation [11]. The two functions of FLP-11 might mechanistically
565 separate at the level of divergent receptors, signaling pathways or cell types downstream
566 of FLP-11 that mediate either the sleep or the survival response. For example, the receptors
567 and downstream cell types that mediate the effects of FLP-11 on dampening wakefulness
568 circuits might desensitize quickly, thus limiting the amount of behavioral sleep that can be
569 induced by FLP-11 released from RIS. Along these lines, RIS activity might exert a
570 survival-promoting effect through a mechanism with different desensitization properties.
571 Survival appears to be a function of RIS activity, depends on *flp-11*, but does not seem to
572 depend on activation transients. Thus, the underlying signaling components do not seem to
573 desensitize quickly but might respond to lower levels of RIS activity or might integrate
574 RIS activity over time. This could hypothetically be achieved by FLP-11 activating
575 downstream receptors and cell types that react sensitively to FLP-11 concentration, that do
576 not easily desensitize and that promote survival upon sensing FLP-11. The key FLP-11
577 receptors required for promoting sleep and survival and the cells in which these receptors
578 function have not yet been identified [11]. The identification of FLP-11 receptors will
579 allow for further studies of the mechanisms by which FLP-11 causes sleep behavior and
580 survival. Another hypothetical explanation for changes in sleep behavior upon expression
581 of ion channel mutants might be changes in the underlying neuronal connectivity. Further
582 experimentation is required to test these speculative hypotheses.
583
584 What is the mechanism and role of homeostatic compensation during sleep deprivation?
585 Homeostatic regulation can compensate for lost or disturbed sleep across species and plays
586 an important role in the regulation of sleep in *C. elegans* [22, 53, 67, 69, 73]. The typical
587 effects of disturbing sleep or depriving an animal of sleep are a reduction of sleep behavior
588 caused by continued activity of wakefulness circuits that steer behavioral activity.
589 Increased behavioral activity is often accompanied by a subsequent overactivation of sleep-
590 active neurons that promote a rebound phase of increased sleep duration or intensity.
591 Rebound sleep in turn is thought to compensate for lost or disturbed sleep, at least partially
592 [8, 22, 24, 67, 69, 73, 74].
593

How is *RIS::unc-58gf(strong)* related to sleep deprivation and sleep homeostasis? Does *RIS::unc-58gf(strong)* trigger homeostatic compensation of the lost sleep? Does the transgene cause a state that is similar to the effects of sleep-deprivation? To answer these questions, we first studied behavioral sleep across stages. Across the life of arrested larvae, behavioral quiescence was reduced in *RIS::unc-58gf(strong)*. Furthermore, sleep was reduced by *RIS::unc-58gf(strong)* during L1 lethargus and after stress in the adult. We also studied the activity of excitable cells in *RIS::unc-58gf(strong)* in arrested L1 larvae. We studied the activity of sensory neurons, interneurons and body wall muscle. All of these excitable cells are known to be rather inactive during sleep and thus the study of the activity of these excitable cells allows for a quantitative description of sleep depth. Our data showed that the sleep bouts in *RIS::unc-58gf(strong)* are less pronounced and hence appear to be less deep. Hence we could not find any signs of deeper or compensatory sleep in *RIS::unc-58gf(strong)*. By contrast, the analysis of excitable cells suggested that the residual bouts of behavioral quiescence in *RIS::unc-58gf(strong)* were generally weakened. *RIS::unc-58gf(strong)* thus displays the neuronal signature of sleep deprivation or disturbed sleep, i.e. the combination of impaired wakefulness circuit dampening and over activation of RIS. Thus, *RIS::unc-58gf(strong)* might be understood and employed as a model of disturbed sleep or of sleep deprivation.

Does RIS activate when the animals are disturbed to promote survival [12, 18, 22, 24, 69]? To further illustrate the idea of RIS acting as a promoter of survival, we disturbed animals during sleep via a lethal blue-light stimulus. Lethal blue light increased RIS activity and functional RIS was required for extending the survival of the animals during blue-light stimulation yet did not increase sleep behavior. This supports the idea that RIS activates upon sensory stimulation to promote survival independently of increasing sleep behavior.

What is the mechanism by which RIS promotes survival? Is there an important role of RIS to conserve energy by shutting down behavior? The reduction of brain and muscle activity likely contributes to survival by conserving energy. While energy consumption appears to be playing a role in survival, behavioral activity and thus energy consumption does not correlate with survival when transmission from RIS is strongly increased. In *RIS::unc-*

625 *58gf(strong)* animals, neuronal, muscle and behavioral activity are high and consume
626 energy, yet survival is increased. Hence RIS appears to be able to promote survival
627 independently of sleep behavior and despite the energy loss that can be expected to be
628 caused by the increased activity of excitable cells [28]. As both sleep and survival are
629 functions of RIS activity over a wide range of conditions, the two processes should be
630 coupled during normal sleep. During each sleep bout, RIS depolarizes and thus should
631 promote both, sleep and survival. Such coupling of sleep and survival during normal sleep
632 might ensure that phases of brain and behavioral inactivity coincide with phases during
633 which survival-promoting processes are active. Tight coupling might serve to optimize
634 energy expenditure, as energy conserved by sleep could be directly allocated to survival-
635 promoting processes [28].
636
637 How does RIS cause physiological protection and increased survival independently of
638 conserving energy? RIS promotes survival of stressful conditions and underlying changes
639 in protective gene expression [12, 18, 24]. Together with the apparent strong reduction of
640 sleep behavior in *RIS::unc-58gf(strong)*, this might suggest that the role of RIS
641 overactivation upon disturbance or sleep deprivation is not only to promote rebound sleep
642 behavior, but also to promote protective physiological benefits that support survival. An
643 important function of RIS might thus be to promote survival when the animal is disturbed
644 by sensory stimulation. Disturbance, e.g. by blue light, might directly be stressful and thus
645 require an increased survival response. Disturbed sleep is often associated with stress, for
646 example when mechanical stimuli are experienced. Hence RIS might hypothetically also
647 act as part of a sensory system that activates during stimulation to signal an increased
648 demand of physiological protection.
649
650 The FOXO transcription factor DAF-16 has been shown to be linked to the control and
651 functions of sleep. It is required for sleep under various conditions including during L1
652 arrest. Also, FOXO has been shown to be activated upon sleep deprivation during both
653 lethargus as well as during L1 arrest and to be required for increased rebound sleep
654 following sleep disturbances [24, 58, 67, 73] (Fig S10). A plausible model hence suggests
655 that RIS activation promotes DAF-16-dependent gene expression changes in order to

support survival [24]. Our data indicate that RIS strongly promotes protective gene expression despite the loss of sleep behavior. Thus, *RIS::unc-58gf(strong)* intensifies the survival function of RIS while inhibiting the sleep function of RIS.

By controlling the activity of RIS, we showed that the survival function and the sleep behavior function of this neuron can be decoupled. By constantly elevating RIS baseline activity, we generated a condition in which wakefulness neural activity and sleep-active neuron activity coexist. A similar condition often underlies disturbed sleep. Our data suggest that when sleep is disturbed, RIS promotes survival despite the loss of behavioral sleep. It would be interesting to study whether sleep neurons in other species also can promote physiological benefits in the face of lost sleep.

668 **Materials and Methods**

669

670 **Resource and Materials Availability**

671 Key *C. elegans* lines that were used in this project are available at the Caenorhabditis
672 elegans Genetics Center. Other *C. elegans* strains, plasmids, or additional reagents
673 generated for this study are available upon reasonable request.

674

675 **Data Availability**

676 All relevant data are within the manuscript and its supporting Information files. Matlab
677 scripts can be found at Github (https://github.com/ibusack/A-sleep-active-neuron-can-
678 promote-survival-while-sleep-behavior-is-disturbed).

679

680 **Experimental model and subject details**

681 *C. elegans* hermaphrodites were maintained at 20°C. They were kept on Nematode Growth
682 Medium Plates (NGM). The *Escherichia coli* strain OP50 served as a food source during
683 maintenance [75].

684

685 **Method Details**

686

687 **Crossing *C. elegans* strains**

688 Males were generated via heat shock or maintained by a continuation of crossings of
689 worms of the same genotype [76]. Single worms of the F2 generation were genotyped
690 using duplex PCR genotyping [77]. For crossing fluorescent transgenes, fluorescent
691 markers were used. All strains and primers of this study can be found in the
692 supplementary tables S2 and S3.

693

694 **Creating mutants with the CRISPR/Cas9 system**

695 We designed the sequences of the following transgenes in silico. Transgenes were
696 synthesized and inserted into the genome by using CRISPR/Cas9 by SunyBiotech.
697 Transgene sequences were verified by Sanger sequencing.

PHX1433	*flp-11(syb1433 [flp-11-SL2-egl-23cDNA(A383V)-linker-mKate2]) X*
PHX1445	*aptf-1(gk794) II; flp-11(syb1445[flp-11-SL2-unc-58(L428F)-linker-mKate2]) X*
PHX1464	*flp-11(syb1464[flp-11-SL2-egl-23cDNA(L229N)-linker-mKate2]) X*
PHX2193	*flp-11(syb2193[flp-11b-SL2(gpd-2)-mKate2-linker-twk-18(e1913)]) X*
PHX2493	*lgc-38(syb2346[flp-11p::dpy-10 site::flp-11 3'UTR], syb2493[ReaChR-linker*-mKate2]) III.
PHX3190	*lgc-38(syb2346[flp-11p::dpy-10 site::flp-11 3'UTR] ,syb3190[unc-58(e665)-linker(GSGSGSGSG)-mKate2]) III*
PHX4110	*lgc-38(syb2346[flp-11p::dpy-10 site::flp-11 3'UTR], syb4110[unc-58gf-CAI-1.0-linker(GSGSGSGSG)-mKate2]) III*
PHX4416	*aptf-1(gk794) II; flp-11(syb1445 syb4416) X*

The coding sequences of the ion channel transgenes were synthesized and consisted each of the spliced coding sequence of the ion channel including the mutation that caused the leak current [32], a nine amino acid long C-terminal linker sequence (GSGSGSGSG) followed by a C-terminal mKate2 gene. The coding sequence of mKate2 was codon optimized and two introns were inserted [78]. The coding sequences of the ion channels were not codon optimized to allow for proper folding of the membrane proteins. We tried codon-optimization [78] of the *unc-58(L428F)* channel gene and mKate2 to achieve high expression, but this also caused aggregation of the fluorescent fusion protein (Fig S1A, D). Hence, we used the endogenous gene sequence for the channel and only codon-optimized mKate2. The sequences of the ion channel transgenes can be found in the supplemental information.

Analysis of the RIS transcriptome showed that *flp-11* has the strongest and most specific promoter of all RIS-expressed genes, with 157-fold higher expression in RIS than in other neurons [17]. *flp-11* is also expressed in other neurons, albeit at low levels [11, 17, 31]. Using imaging settings that cause oversaturation of the mKate2 signal in RIS revealed that there is a weak expression of *unc-58gf::mKate2* in a few neurons in the ventral cord in

728 *RIS::unc-58gf(strong)* (Fig S1F). Expression from the *flp-11* promoter in RIS but not in
729 other neurons depends on *aptf-1* [11]. We hence imaged mKate2 expression in *aptf-1(-).*
730 Consistent with previous results [11], mKate2 expression was abolished in RIS but was
731 still present in the ventral cord (Fig S1G). Thus, expression from the *flp-11* promoter is
732 strong, has a high level of RIS specificity, and RIS expression depends on *aptf-1*.

733

734 The sequences of the ion channels of the strains PHX1433, PHX1445, PHX1464 and
735 PHX2193 were inserted after the stop codon of the *flp-11* endogenous coding sequence
736 together with an SL2 site. Thus, an operon was created that expressed both *flp-11* and the
737 ion channel gene from the *flp-11* promoter. The transgenes of PHX2493, PHX3190 and
738 PHX4110 were generated via a single-copy knock-in loci for defined gene expression (SKI
739 LODGE) system [34]. For the SKI LODGE expression in RIS we first inserted the minimal
740 *flp-11* 3' and 5'UTRs separated by a *dpy-10* sgRNA cutting site. The expression from these
741 minimal UTR sequences allowed specific expression in RIS, but the expression levels were
742 lower compared with the endogenous *flp-11* locus (Fig 1A-D, S1A-D). The final sequences
743 of all transgenes can be found in the supplementary Text S1.

744

745 **Imaging using microfluidic devices**

746 Worms were filmed in microfluidic devices made from agarose hydrogel as previously
747 described [37, 38]. In brief, a PDMS mold was used to cast box-shaped indentations from
748 melted 5% agarose diluted in M9 buffer. After agarose hydrogel solidification the stamp
749 was removed resulting in hundreds of microchambers sized 110x110x10µm for L1 arrest
750 chambers or 190x190x15µm for L1 lethargus chambers per agarose slab. Depending on
751 the experiment, approximately 9-36 pretzel-stage eggs per strain were then transferred
752 without food for L1 arrest or with food for lethargus into the indentations in the hydrogel
753 and the chambers were closed with a coverslip and kept in a temperature-controlled dish.
754 Hatching of the larvae in the absence of food caused L1 arrest. Chambers were timed so
755 that the worms were incubated for 48h at 25°C before imaging. The number of biological
756 replicates (n) imaged in microfluidic devices is stated in each figure. One or several
757 technical replicates (different microfluidic devices) were imaged for each experiment.

758

759 **Software for imaging**

760 All image acquisition was performed with Nikon NIS Elements 5 software (Nikon,
761 Tokyo).

762

763 **Dark Differential Contrast (DIC) Imaging**

764 Long-term dark differential contrast (DIC) images were acquired with a standard 100W
765 halogen lamp and an infrared filter (Semrock Brightline HC 785/62) (Idex Health and
766 Science, New York). The images for L1 arrest imaging were taken 48h upon starvation for
767 12h with a frame rate of 0.1Hz. A 20x objective for imaging was combined with a 0.7 lens.
768 Lethargus data was acquired with similar settings except the frame rate was 0.2Hz.

769

770 **Functional Ca^{2+}-imaging**

771 For calcium imaging we used either a back-illuminated sCMOS camera (Photometrics
772 Prime 95B, 1200x1200 pixels) (Fig 3, 4, 8C-H, S3) or an Andor iXon EMCCD camera
773 (512x512 pixels, Andor Technology Ltd., Belfast). (Fig 6, 7, 8A-B, S5, S6). The gain of
774 the iXon camera was set to 200. The iXon camera's read out mode was 10MHz at 14-bit.
775 The images of the Photometrics camera were binned 2 x 2.

776

777 A 20x objective was used to simultaneously image 3 x 3 adjacent microchambers
778 containing one worm each (This configuration was used to obtain data for Fig 6, 7, 8A-B,
779 S5, S6). A 10x objective combined with a 1.5x lens was used to simultaneously image 6 x
780 6 adjacent microchambers containing one worm each (this configuration was used to obtain
781 data for Fig 3, 4, 8C-H, S3).

782

783 For calcium imaging we utilized a 480nm LED and a standard GFP filter set (EGFP,
784 Chroma). The EMCCD camera TTL signal triggered the LED. The 490nm intensities were
785 set to either 0.23mW/mm^2 with an exposure time of 50ms (Fig 3A, 4A-H, 8C-H),
786 0.33mW/mm^2 (Fig 6A-D) or 0.51 mW/mm^2 (Fig 6E-H), both with an exposure time of
787 5ms or 0.33mW/mm^2 with an exposure time of 10ms (PLM). Additional mKate2
788 fluorescence images were acquired for the RIS, RIM and PLM activity experiments. For

789 this measurement we used a 585nm LED and a set of standard Texas Red filters (Chroma).
790 The 585nm LED intensity was set to 0.11mW/mm^2 while imaging with a 50ms exposure
791 time (RIS) and to 0.15 mW/mm^2 for acquiring images with a 100ms exposure time (RIM,
792 PLM). Calcium and mKate2 imaging were carried out with a frame rate of 0.1Hz for 3h.
793 As the ion channels were additionally tagged with an mKate2, the parental strains without
794 the GCaMP/mKate2 construct were imaged with the same settings with the 585nm LED.
795 Here, no signal could be observed in the parental strains.
796
797 For the long-term calcium imaging from day 1 to day 12 we utilized slightly different LED
798 light intensities. Here, the 490nm intensity was set to 0.34mW/mm^2 and the 585nm light
799 had an intensity of 0.21mW/mm^2.
800
801 **Optogenetic activation**
802 For optogenetic RIS activation experiments, the agarose containing the microchambers
803 was supplemented with 10µl of 10mM all-trans-retinal (ATR, Sigma Aldrich) dissolved in
804 ethanol 1h before the start of image acquisition. In experiment in Fig 9, A baseline of
805 GCaMP images was recorded for 1min with a frame rate of 0.33Hz. This was followed by
806 a stimulation phase of 1min, in which again GCaMP images were acquired with a frame
807 rate of 0.33Hz. In between the camera exposures, the worms were illuminated with 585nm
808 LED light with an intensity of 0.17mW/mm^2 for 800ms triggered by the software. After
809 the stimulation period, a recovery period of 1min was imaged, in which GCaMP images
810 were acquired with a frame rate of 0.33Hz. The 490nm LED intensities for imaging were
811 set to 0.39mW/mm^2 and images were acquired with an exposure time of 5ms.
812
813 For the long-term optogenetic imaging worms (Fig 10), a stimulation phase of 11h was
814 recorded in which GCaMP images were acquired with a frame rate of 0.33Hz. In between
815 the camera exposures, the worms were illuminated with 585nm LED light with an intensity
816 of 0.17mW/mm^2 for 800ms triggered by the software.
817
818 **Quantification of expression of mKate2 of the RIS activity strains**

819 Larvae were synchronized via bleaching [17] and hatched in M9 buffer at 25°C. Imaging
820 of most strains was performed after 48h in the L1 arrest stage by transferring worms with
821 a 10 µl liquid drop onto an agarose pad (5% agarose solved in M9 buffer). The *RIS::unc-*
822 *58gf and flp-11(-)* worms were imaged 24h after bleaching. Larvae were then fixed through
823 the addition of 10 µl of 25mM levamisole (Sigma Aldrich).
824
825 To image the expression levels of the different RIS activity transgenes, mKate2 was
826 imaged with an Andor Revolution disc system (Andor Technology Ltd.) and a CSU-X1
827 spinning disc head (Yokogawa). The 561nm laser light intensity was set to 0.49mW/mm^2.
828 The worms were imaged through a 100x oil objective and by an Andor iXon Ultra EMCCD
829 camera (1024x1024 pixels) (Andor Technology Ltd., Belfast). An EM gain of 200 was
830 included and the camera read-out time was set to 30MHz. A z-stack of 21planes, each
831 0.5µm apart (10µm in total) was acquired. For comparison, a maximum z-stack projection
832 was calculated.
833
834
835 **DIC image analysis**
836 Mobility of worms was analyzed from DIC images though image subtraction as previously
837 described [17, 79]. The matrix of intensity values of the preceding image was subtracted
838 from the matrix of intensity of the following image. A mean of all values of the difference
839 matrix was then calculated to attain a mean smoothed image subtraction value, which
840 represents the movement of the worm.
841
842 To identify lethargus in fed worms, the non-pumping time prior to molting was identified.
843 For the sleep analysis in recovery lethargus after 12 days of starvation followed by
844 refeeding, 3h prior to molt were analyzed for mobility quiescence.
845
846 **Analyzing functional Ca^{2+}-images**
847 Neuronal intensities were automatically analyzed via custom-written MATLAB scripts
848 that are available at Github (https://github.com/ibusack/A-sleep-active-neuron-can-
849 promote-survival-while-sleep-behavior-is-

850 disturbed/blob/main/analysisfluorescentsignal.m). These codes extracted the regions of
851 interest through an intensity threshold and acquired the intensities and position data. The
852 extracted regions were set to be slightly bigger than the actual size of the neuron to allow
853 for background intensity detection and background subtraction. The pan-neuronal activity
854 was measured treating the head neurons as a combined signal. The RIS GCaMP activity in
855 Figure 6 was determined by extracting the position data of the corresponding mKate2
856 signal. A larger region of interest was extracted and a fitting percentage of that was
857 calculated as the signal. The extracted position data of the signal served to calculate the
858 speed values.
859
860 RIS, RIM and PLM activities were normalized by dividing GCaMP intensities through
861 corresponding mKate2 intensities. In the optogenetic experiment, the baseline
862 measurements were used for normalization.
863
864 **Mobility quiescence detection**
865 First, speeds or image subtraction mean intensities were smoothed over 30 time points
866 through the *smooth* function in MATLAB, which is a first-degree polynomial local
867 regression model. The code is available at Github (https://github.com/ibusack/A-sleep-
868 active-neuron-can-promote-survival-while-sleep-behavior-is-
869 disturbed/blob/main/boutdetection.m). Smoothed speeds and image subtraction values
870 were normalized between 0 and 1 for each individual animal with 0 being the lowest speed
871 value and 1 the highest speed value the animal possessed. A mobility quiescence bout was
872 counted when the normalized speed was below a specific percentage for a certain amount
873 of time. For calcium imaging experiments with the 20x objective (Fig 6), the normalized
874 speed had to be below 10% for at least 3min. The RIS activity experiment, which was
875 filmed with a 10x objective, required a percentage threshold of 5% for a minimum of 4min.
876 For DIC images filmed with the 20x objective, the normalized mean image subtraction
877 values had to be below 15% for at least 3min to be counted as sleep time points. The code
878 for detecting sleep bouts based on RIM tracking can be found at Github
879 (https://github.com/ibusack/A-sleep-active-neuron-can-promote-survival-while-sleep-
880 behavior-is-disturbed/blob/main/RIM_sleepboutdetection.m.)

881

882 **Mobility quiescence bout onset alignment**

883 Speeds and GCaMP intensities were aligned to the start of mobility quiescence bouts,
884 which had been detected by the mobility quiescence bout analysis. Mobility quiescence
885 bouts were only counted for the alignment when the worm was mobile throughout 3min
886 prior to the mobility quiescence bout onset. This alignment was carried out with a custom-
887 written MATLAB script which is published on Github (https://github.com/ibusack/A-
888 sleep-active-neuron-can-promote-survival-while-sleep-behavior-is-
889 disturbed/blob/main/boutdetection.m).

890

891 **Neuronal inactivity detection**

892 The neuronal activities were treated similarly as speed values for the mobility quiescence
893 detection. Hence the boutdetection MATLAB script was utilized, which can be found on
894 Github (https://github.com/ibusack/A-sleep-active-neuron-can-promote-survival-while-
895 sleep-behavior-is-disturbed/blob/main/boutdetection.m).
896 The nervous system was counted as inactive when it was below 20% of the smoothed and
897 normalized activity for at least 3min.

898

899 **RIM neuron inactivity detection**

900 RIM peaks were detected through a custom-written MATLAB script, which is available at
901 Github (https://github.com/ibusack/A-sleep-active-neuron-can-promote-survival-while-
902 sleep-behavior-is-disturbed/blob/main/analyze_RIM.m). First, the activity values were
903 smoothed using the inbuilt *smooth* function over 5 time points. Then, peaks of a minimum
904 prominence of 0.2 were extracted via the inbuilt function *islocalmax.* RIM was counted as
905 inactive when there were no detected peaks for at least 5min.

906

907 **Induction of cellular stress by heat shock**

908 The heat shock was carried out following a previously described protocol and utilizing a
909 previously described heat shock device [17]. To summarize, young adult worms were
910 imaged in 370x370x45µm microfluidic chambers and for a total of 4h. 5 to 12 worms were
911 transferred from plates grown at 20°C to the microchamber. The worms were starved for

912 90min at 20°C before filming. During the entire duration of the movie, DIC images were
913 acquired at a frequency of 0.1Hz. First, a baseline was recorded for 1h with the sample
914 holder temperature set to 22°C and the heating lid set to 25°C. Then the heat shock was
915 conducted with the sample holder temperature set to 37°C and the heating lid set to 39°C
916 for 20 minutes. Finally, a recovery phase was recorded with the sample holder temperature
917 set to 22°C and the heating lid set to 25°C for 2h 40min.
918
919 **Pumping assay**
920 Arrested L1 worms were imaged in 110x110x10µm microfluidic chambers. DIC images
921 were acquired with a frequency of 10 Hz for 1min. Pumps of the grinder were then
922 counted manually with the help of a clicker.
923
924 **Survival assay in liquid culture**
925 RIS impairment has been shown to confer a reduction of survival in both liquid culture and
926 in microfluidic chambers [12, 23, 24, 36]. Worms were synchronized by bleaching [17]. 3-
927 4 days before bleaching, 10-12 L4 stage worms were transferred onto NGM plates with a
928 diameter of 6cm. 1-2 plates were bleached per strain and the day of bleaching was defined
929 as day 0. The worms were kept in 1ml of M9 buffer in 2ml Eppendorf tubes in a rotator at
930 20°C for most survival assays. The following day was counted as day 1 of the lifespan.
931 During the survival assay, the worms were kept in liquid culture in 1ml M9 buffer in 2ml
932 Eppendorf tubes. This resulted in a population density of approximately 100 worms per
933 10µl. The tubes were placed in a rotator at 20°C, which rotated at 20rpm. For counting,
934 10µl drops of the liquid culture were pipetted onto fresh NGM plates for each strain
935 respectively. The worms were allowed to recover for at least 2h after pipetting before
936 counting. Counting was performed manually with the assistance of a clicker. The recovery
937 number, i.e., the number of worms that developed into at least the L4 stage, was counted
938 3-5 days after pipetting. Around 50-100 worms were counted for each strain of each
939 replicate on each time point.
940
941 **Survival assay in the OptoGenBox**

942 For the long-term optogenetic survival assay worms were kept in microfluidic chambers
943 (110x110x15µm) as described above. Between 27 and 43 worms were used for each strain
944 per agarose slab each containing many microfluidic chambers. A maximum of one worm
945 was placed per microfluidic chamber. Three replicates were performed per condition. We
946 then calculated the average of all individuals of all three replicates combined. For the
947 optogenetic activation 10µl of 10mM all-trans-retinal (ATR, Sigma Aldrich) dissolved in
948 ethanol was added every 3-4 days. 20µl of 10µg/ml nystatin dissolved in DMSO was added
949 3-4 times throughout the lifespan to prevent fungal contamination. To prevent drying out
950 of the agarose, 20µl of sterile water was added every 2 days. In the first week, the worms
951 were counted every second day, then the survival was counted every day until all worms
952 had died. A worm was counted as dead if a 2 min blue-light stimulus did not cause a visible
953 behavioral response.
954
955 For long-term optogenetic activation of RIS, worms were placed in the OptoGenBox [23]
956 and continuously illuminated with 10mW at 20°C.
957
958 **Blue light survival assay**
959 For the blue-light survival assays worms were imaged in 110x110x10µm microchambers.
960 A blue light stimulus of 0.74mW/mm^2 was given for 1s every 5s while simultaneously
961 taking a GCaMP image. For the control, the same intensity stimulus was given for only
962 100ms through the camera exposure time.
963
964 **Imaging of growing worms**
965 The images of growing plates were taken at a Leica M125 stereomicroscope. A Jenoptik
966 ProgRes MF captured the images utilizing the corresponding software ProgResCapturePro
967 2.10.0.1.
968
969 **RNA sequencing data**
970 RNA sequencing data is described in [24].
971
972 **Fitting**

973 Origin software was used for the regression analyses. A linear regression was fitted to the
974 data in Figure 6C and 6G. R^2 values can be found in the corresponding figures. The exact
975 functions are in Table 1.
976

Figure panel	fit	function
6C	linear	$y = 0.116 + 0.5494x$
6G	linear	$y = 0.21203 + 1.10949x$

977 Table 1. Calculated functions for the regressions.
978

979 **Quantification and Statistical Analysis**

980 The experimenter was blind to the genotype information during the lifespan experiments.
981 All other experiments relied on an automated analysis and hence were not blinded. The
982 Wilcoxon signed rank test was utilized for the comparison of speeds and GCaMP
983 intensities within the same strain. The Welch test was conducted to compare data from
984 different strains. The survival assay experiments were statistically analyzed by utilizing the
985 Fisher's exact test at 50% survival of the wild type. Experiments with four or more
986 genotypes were FDR corrected by the Benjamini-Hochberg procedure with a 5% false
987 discovery rate. The graphs depict the mean and standard error of the mean. Box plots
988 display individual data points, the interquartile range and the median. The whiskers
989 represent the 10-90th percentile. A table listing all exact p-values can be found in the
990 supplemental information (Table S4).
991

992 **Acknowledgements**

993 Some strains were provided by the CGC, which is funded by NIH Office of Research
994 Infrastructure Programs (P40 OD010440). The CRISPR strains were generated by
995 SunyBiotech based on our design. We thank Thomas Boulin for communicating the sodium
996 permeability of *unc-58gf* and suggesting its use as a tool for neuronal activation. This work
997 was supported by a European Research Council Starting Grant (ID: 637860,
998 SLEEPCONTROL).
999

1000 **Author contributions**

I.B.: Data curation, Formal analysis, Investigation, Methodology, Project administration, Resources, Software, Visualization, Writing – review & editing.

H.B.: Conceptualization, Funding acquisition, Investigation, Methodology, Project administration, Resources, Supervision, Writing – original draft.

Declaration of Interest

The authors declare no competing interests.

1008 **References**

1009

1010 1. Campbell SS, Tobler I. Animal sleep: a review of sleep duration across
1011 phylogeny. Neurosci Biobehav Rev. 1984;8(3):269-300. Epub 1984/01/01. PubMed
1012 PMID: 6504414.
1013 2. Diekelmann S, Born J. The memory function of sleep. Nature reviews
1014 Neuroscience. 2010;11(2):114-26. Epub 2010/01/05. doi: 10.1038/nrn2762. PubMed
1015 PMID: 20046194.
1016 3. Krueger JM, Frank MG, Wisor JP, Roy S. Sleep function: Toward elucidating an
1017 enigma. Sleep medicine reviews. 2016;28:46-54. Epub 2015/10/09. doi:
1018 10.1016/j.smrv.2015.08.005. PubMed PMID: 26447948; PubMed Central PMCID:
1019 PMC4769986.
1020 4. Anafi RC, Kayser MS, Raizen DM. Exploring phylogeny to find the function of
1021 sleep. Nature reviews Neuroscience. 2019;20(2):109-16. Epub 2018/12/24. doi:
1022 10.1038/s41583-018-0098-9. PubMed PMID: 30573905.
1023 5. Hublin C, Partinen M, Koskenvuo M, Kaprio J. Sleep and mortality: a population-
1024 based 22-year follow-up study. Sleep. 2007;30(10):1245-53. Epub 2007/11/01. doi:
1025 10.1093/sleep/30.10.1245. PubMed PMID: 17969458; PubMed Central PMCID:
1026 PMCPMC2266277.
1027 6. Van Cauter E, Spiegel K, Tasali E, Leproult R. Metabolic consequences of sleep
1028 and sleep loss. Sleep Med. 2008;9 Suppl 1:S23-8. Epub 2008/12/17. doi: 10.1016/S1389-
1029 9457(08)70013-3. PubMed PMID: 18929315; PubMed Central PMCID:
1030 PMCPMC4444051.
1031 7. Irwin MR. Why sleep is important for health: a psychoneuroimmunology
1032 perspective. Annu Rev Psychol. 2015;66:143-72. Epub 2014/07/26. doi:
1033 10.1146/annurev-psych-010213-115205. PubMed PMID: 25061767; PubMed Central
1034 PMCID: PMCPMC4961463.
1035 8. Saper CB, Fuller PM, Pedersen NP, Lu J, Scammell TE. Sleep state switching.
1036 Neuron. 2010;68(6):1023-42. Epub 2010/12/22. doi: 10.1016/j.neuron.2010.11.032.
1037 PubMed PMID: 21172606; PubMed Central PMCID: PMC3026325.
1038 9. Bringmann H. Sleep-Active Neurons: Conserved Motors of Sleep. Genetics.
1039 2018;208(4):1279-89. Epub 2018/04/06. doi: 10.1534/genetics.117.300521. PubMed
1040 PMID: 29618588; PubMed Central PMCID: PMC5887131.
1041 10. Turek M, Lewandrowski I, Bringmann H. An AP2 transcription factor is required
1042 for a sleep-active neuron to induce sleep-like quiescence in C. elegans. Curr Biol.
1043 2013;23(22):2215-23. Epub 2013/11/05. doi: 10.1016/j.cub.2013.09.028. PubMed PMID:
1044 24184105.
1045 11. Turek M, Besseling J, Spies JP, Konig S, Bringmann H. Sleep-active neuron
1046 specification and sleep induction require FLP-11 neuropeptides to systemically induce
1047 sleep. eLife. 2016;5. Epub 2016/03/08. doi: 10.7554/eLife.12499. PubMed PMID:
1048 26949257; PubMed Central PMCID: PMC4805538.
1049 12. Wu Y, Masurat F, Preis J, Bringmann H. Sleep Counteracts Aging Phenotypes to
1050 Survive Starvation-Induced Developmental Arrest in C. elegans. Curr Biol.
1051 2018;28(22):3610-24 e8. Epub 2018/11/13. doi: 10.1016/j.cub.2018.10.009. PubMed
1052 PMID: 30416057; PubMed Central PMCID: PMCPMC6264389.

1053 13. Skora S, Mende F, Zimmer M. Energy Scarcity Promotes a Brain-wide Sleep
1054 State Modulated by Insulin Signaling in C. elegans. Cell reports. 2018;22(4):953-66.
1055 Epub 2018/02/02. doi: 10.1016/j.celrep.2017.12.091. PubMed PMID: 29386137.
1056 14. Gonzales DL, Zhou J, Fan B, Robinson JT. A microfluidic-induced C. elegans
1057 sleep state. Nat Commun. 2019;10(1):5035. Epub 2019/11/07. doi: 10.1038/s41467-019-
1058 13008-5. PubMed PMID: 31695031.
1059 15. Steuer Costa W, Van der Auwera P, Glock C, Liewald JF, Bach M, Schuler C, et
1060 al. A GABAergic and peptidergic sleep neuron as a locomotion stop neuron with
1061 compartmentalized Ca2+ dynamics. Nat Commun. 2019;10(1):4095. Epub 2019/09/12.
1062 doi: 10.1038/s41467-019-12098-5. PubMed PMID: 31506439.
1063 16. Grubbs JJ, Lopes LE, van der Linden AM, Raizen DM. A salt-induced kinase is
1064 required for the metabolic regulation of sleep. PLoS biology. 2020;18(4):e3000220. Epub
1065 20200421. doi: 10.1371/journal.pbio.3000220. PubMed PMID: 32315298; PubMed
1066 Central PMCID: PMCPMC7173979.
1067 17. Konietzka J, Fritz M, Spiri S, McWhirter R, Leha A, Palumbos S, et al. Epidermal
1068 Growth Factor Signaling Promotes Sleep through a Combined Series and Parallel Neural
1069 Circuit. Curr Biol. 2020;30(1):1-16 e3. Epub 2019/12/17. doi:
1070 10.1016/j.cub.2019.10.048. PubMed PMID: 31839447.
1071 18. Sinner MP, Masurat F, Ewbank JJ, Pujol N, Bringmann H. Innate Immunity
1072 Promotes Sleep through Epidermal Antimicrobial Peptides. Curr Biol. 2021;31(3):564-77
1073 e12. Epub 2020/12/02. doi: 10.1016/j.cub.2020.10.076. PubMed PMID: 33259791.
1074 19. Makino M, Ulzii E, Shirasaki R, Kim J, You YJ. Regulation of Satiety
1075 Quiescence by Neuropeptide Signaling in Caenorhabditis elegans. Front Neurosci.
1076 2021;15:678590. Epub 2021/08/03. doi: 10.3389/fnins.2021.678590. PubMed PMID:
1077 34335159; PubMed Central PMCID: PMCPMC8319666.
1078 20. Nichols ALA, Eichler T, Latham R, Zimmer M. A global brain state underlies C.
1079 elegans sleep behavior. Science. 2017;356(6344). Epub 2017/06/24. doi:
1080 10.1126/science.aam6851. PubMed PMID: 28642382.
1081 21. Xu Y, Zhang L, Liu Y, Topalidou I, Hassinan C, Ailion M, et al. Dopamine
1082 receptor DOP-1 engages a sleep pathway to modulate swimming in C. elegans. iScience.
1083 2021;24(4):102247. Epub 2021/04/03. doi: 10.1016/j.isci.2021.102247. PubMed PMID:
1084 33796839; PubMed Central PMCID: PMCPMC7995527.
1085 22. Maluck E, Busack I, Besseling J, Masurat F, Turek M, Busch KE, et al. A wake-
1086 active locomotion circuit depolarizes a sleep-active neuron to switch on sleep. PLoS
1087 biology. 2020;18(2):e3000361. Epub 2020/02/23. doi: 10.1371/journal.pbio.3000361.
1088 PubMed PMID: 32078631.
1089 23. Busack I, Jordan F, Sapir P, Bringmann H. The OptoGenBox - a device for long-
1090 term optogenetics in C. elegans. J Neurogenet. 2020:1-9. Epub 2020/06/17. doi:
1091 10.1080/01677063.2020.1776709. PubMed PMID: 32543249.
1092 24. Koutsoumparis A, Welp LM, Wulf A, Urlaub H, Meierhofer D, Börno S, et al.
1093 Sleep neuron depolarization promotes protective gene expression changes and FOXO
1094 activation. Current Biology. 2022. doi: https://doi.org/10.1016/j.cub.2022.04.012.
1095 25. Kenyon CJ. The genetics of ageing. Nature. 2010;464(7288):504-12. Epub
1096 2010/03/26. doi: 10.1038/nature08980. PubMed PMID: 20336132.
1097 26. Baugh LR, Hu PJ. Starvation Responses Throughout the Caenorhabditis elegans
1098 Life Cycle. Genetics. 2020;216(4):837-78. Epub 2020/12/04. doi:

1099 10.1534/genetics.120.303565. PubMed PMID: 33268389; PubMed Central PMCID:
1100 PMCPMC7768255.
1101 27. Siegel JM. Sleep viewed as a state of adaptive inactivity. Nature reviews
1102 Neuroscience. 2009;10(10):747-53. Epub 2009/08/06. doi: 10.1038/nrn2697. PubMed
1103 PMID: 19654581.
1104 28. Schmidt MH. The energy allocation function of sleep: a unifying theory of sleep,
1105 torpor, and continuous wakefulness. Neurosci Biobehav Rev. 2014;47:122-53. Epub
1106 2014/08/15. doi: 10.1016/j.neubiorev.2014.08.001. PubMed PMID: 25117535.
1107 29. Krause AJ, Simon EB, Mander BA, Greer SM, Saletin JM, Goldstein-Piekarski
1108 AN, et al. The sleep-deprived human brain. Nature reviews Neuroscience.
1109 2017;18(7):404-18. Epub 2017/05/19. doi: 10.1038/nrn.2017.55. PubMed PMID:
1110 28515433.
1111 30. Klinzing JG, Niethard N, Born J. Mechanisms of systems memory consolidation
1112 during sleep. Nat Neurosci. 2019;22(10):1598-610. Epub 2019/08/28. doi:
1113 10.1038/s41593-019-0467-3. PubMed PMID: 31451802.
1114 31. Taylor SR, Santpere G, Weinreb A, Barrett A, Reilly MB, Xu C, et al. Molecular
1115 topography of an entire nervous system. Cell. 2021. Epub 2021/07/09. doi:
1116 10.1016/j.cell.2021.06.023. PubMed PMID: 34237253.
1117 32. Ben Soussia I, El Mouridi S, Kang D, Leclercq-Blondel A, Khoubza L, Tardy P,
1118 et al. Mutation of a single residue promotes gating of vertebrate and invertebrate two-
1119 pore domain potassium channels. Nat Commun. 2019;10(1):787. Epub 2019/02/17. doi:
1120 10.1038/s41467-019-08710-3. PubMed PMID: 30770809; PubMed Central PMCID:
1121 PMCPMC6377628.
1122 33. Kunkel MT, Johnstone DB, Thomas JH, Salkoff L. Mutants of a temperature-
1123 sensitive two-P domain potassium channel. J Neurosci. 2000;20(20):7517-24. doi:
1124 10.1523/JNEUROSCI.20-20-07517.2000. PubMed PMID: 11027209; PubMed Central
1125 PMCID: PMCPMC6772866.
1126 34. Silva-Garcia CG, Lanjuin A, Heintz C, Dutta S, Clark NM, Mair WB. Single-
1127 Copy Knock-In Loci for Defined Gene Expression in Caenorhabditis elegans. G3
1128 (Bethesda). 2019;9(7):2195-8. Epub 2019/05/09. doi: 10.1534/g3.119.400314. PubMed
1129 PMID: 31064766; PubMed Central PMCID: PMCPMC6643881.
1130 35. Bringmann H. Genetic sleep deprivation: using sleep mutants to study sleep
1131 functions. EMBO Rep. 2019;20(3). Epub 2019/02/26. doi: 10.15252/embr.201846807.
1132 PubMed PMID: 30804011; PubMed Central PMCID: PMCPMC6399599.
1133 36. Roux AE, Langhans K, Huynh W, Kenyon C. Reversible Age-Related
1134 Phenotypes Induced during Larval Quiescence in C. elegans. Cell Metab.
1135 2016;23(6):1113-26. Epub 2016/06/16. doi: 10.1016/j.cmet.2016.05.024. PubMed PMID:
1136 27304510.
1137 37. Bringmann H. Agarose hydrogel microcompartments for imaging sleep- and
1138 wake-like behavior and nervous system development in Caenorhabditis elegans larvae. J
1139 Neurosci Methods. 2011;201(1):78-88. Epub 2011/08/02. doi: S0165-0270(11)00418-3
1140 [pii]10.1016/j.jneumeth.2011.07.013. PubMed PMID: 21801751.
1141 38. Turek M, Besseling J, Bringmann H. Agarose Microchambers for Long-term
1142 Calcium Imaging of Caenorhabditis elegans. Journal of visualized experiments : JoVE.
1143 2015;(100):e52742. Epub 2015/07/02. doi: 10.3791/52742. PubMed PMID: 26132740;
1144 PubMed Central PMCID: PMC4544933.

1145 39. Van Buskirk C, Sternberg PW. Epidermal growth factor signaling induces
1146 behavioral quiescence in Caenorhabditis elegans. Nat Neurosci. 2007;10(10):1300-7.
1147 Epub 2007/09/25. doi: 10.1038/nn1981. PubMed PMID: 17891142.
1148 40. Hill AJ, Mansfield R, Lopez JM, Raizen DM, Van Buskirk C. Cellular stress
1149 induces a protective sleep-like state in C. elegans. Curr Biol. 2014;24(20):2399-405.
1150 Epub 2014/09/30. doi: 10.1016/j.cub.2014.08.040. PubMed PMID: 25264259; PubMed
1151 Central PMCID: PMC4254280.
1152 41. Nelson MD, Lee KH, Churgin MA, Hill AJ, Van Buskirk C, Fang-Yen C, et al.
1153 FMRFamide-like FLP-13 neuropeptides promote quiescence following heat stress in
1154 Caenorhabditis elegans. Curr Biol. 2014;24(20):2406-10. Epub 2014/09/30. doi:
1155 10.1016/j.cub.2014.08.037. PubMed PMID: 25264253; PubMed Central PMCID:
1156 PMC4254296.
1157 42. Iannacone MJ, Beets I, Lopes LE, Churgin MA, Fang-Yen C, Nelson MD, et al.
1158 The RFamide receptor DMSR-1 regulates stress-induced sleep in C. elegans. eLife.
1159 2017;6. Epub 2017/01/18. doi: 10.7554/eLife.19837. PubMed PMID: 28094002; PubMed
1160 Central PMCID: PMCPMC5241116.
1161 43. Cassada RC, Russell RL. The dauerlarva, a post-embryonic developmental variant
1162 of the nematode Caenorhabditis elegans. Dev Biol. 1975;46(2):326-42. Epub 1975/10/01.
1163 doi: 0012-1606(75)90109-8 [pii]. PubMed PMID: 1183723.
1164 44. Raizen DM, Zimmerman JE, Maycock MH, Ta UD, You YJ, Sundaram MV, et
1165 al. Lethargus is a Caenorhabditis elegans sleep-like state. Nature. 2008;451(7178):569-
1166 72. Epub 2008/01/11. doi: nature06535 [pii]10.1038/nature06535. PubMed PMID:
1167 18185515.
1168 45. Yemini E, Lin A, Nejatbakhsh A, Varol E, Sun R, Mena GE, et al. NeuroPAL: A
1169 Multicolor Atlas for Whole-Brain Neuronal Identification in C. elegans. Cell.
1170 2021;184(1):272-88 e11. Epub 2020/12/31. doi: 10.1016/j.cell.2020.12.012. PubMed
1171 PMID: 33378642.
1172 46. Piggott BJ, Liu J, Feng Z, Wescott SA, Xu XZ. The neural circuits and synaptic
1173 mechanisms underlying motor initiation in C. elegans. Cell. 2011;147(4):922-33. Epub
1174 2011/11/15. doi: 10.1016/j.cell.2011.08.053. PubMed PMID: 22078887; PubMed Central
1175 PMCID: PMC3233480.
1176 47. Li W, Kang L, Piggott BJ, Feng Z, Xu XZ. The neural circuits and sensory
1177 channels mediating harsh touch sensation in Caenorhabditis elegans. Nat Commun.
1178 2011;2:315. Epub 2011/05/19. doi: 10.1038/ncomms1308. PubMed PMID: 21587232;
1179 PubMed Central PMCID: PMC3098610.
1180 48. McCormick DA, Bal T. Sensory gating mechanisms of the thalamus. Curr Opin
1181 Neurobiol. 1994;4(4):550-6. doi: 10.1016/0959-4388(94)90056-6. PubMed PMID:
1182 7812144.
1183 49. Schwarz J, Lewandrowski I, Bringmann H. Reduced activity of a sensory neuron
1184 during a sleep-like state in Caenorhabditis elegans. Curr Biol. 2011;21(24):R983-4. Epub
1185 2011/12/24. doi: S0960-9822(11)01207-3[pii]10.1016/j.cub.2011.10.046. PubMed
1186 PMID: 22192827.
1187 50. Schwarz J, Bringmann H. Reduced sleep-like quiescence in both hyperactive and
1188 hypoactive mutants of the Galphaq Gene egl-30 during lethargus in Caenorhabditis
1189 elegans. PLoS One. 2013;8(9):e75853. Epub 2013/09/28. doi:

1190 10.1371/journal.pone.0075853. PubMed PMID: 24073282; PubMed Central PMCID:
1191 PMC3779211.
1192 51. Cho JY, Sternberg PW. Multilevel modulation of a sensory motor circuit during
1193 C. elegans sleep and arousal. Cell. 2014;156(1-2):249-60. Epub 2014/01/21. doi:
1194 10.1016/j.cell.2013.11.036. PubMed PMID: 24439380; PubMed Central PMCID:
1195 PMC3962823.
1196 52. Schwarz J, Spies JP, Bringmann H. Reduced muscle contraction and a relaxed
1197 posture during sleep-like Lethargus. Worm. 2012;1(1):12-4. Epub 2012/01/01. doi:
1198 10.4161/worm.19499. PubMed PMID: 24058817; PubMed Central PMCID:
1199 PMC3670164.
1200 53. Iwanir S, Tramm N, Nagy S, Wright C, Ish D, Biron D. The microarchitecture of
1201 C. elegans behavior during lethargus: homeostatic bout dynamics, a typical body posture,
1202 and regulation by a central neuron. sleep. 2013;36(3):385-95. Epub 2013/03/02. doi:
1203 10.5665/sleep.2456. PubMed PMID: 23449971; PubMed Central PMCID: PMC3571756.
1204 54. Tramm N, Oppenheimer N, Nagy S, Efrati E, Biron D. Why do sleeping
1205 nematodes adopt a hockey-stick-like posture? PLoS One. 2014;9(7):e101162. Epub
1206 2014/07/16. doi: 10.1371/journal.pone.0101162. PubMed PMID: 25025212; PubMed
1207 Central PMCID: PMC4099128.
1208 55. Schwartz HT. A protocol describing pharynx counts and a review of other assays
1209 of apoptotic cell death in the nematode worm Caenorhabditis elegans. Nature protocols.
1210 2007;2(3):705-14. doi: 10.1038/nprot.2007.93. PubMed PMID: 17406633.
1211 56. Song BM, Avery L. The pharynx of the nematode C. elegans: A model system for
1212 the study of motor control. Worm. 2013;2(1):e21833. doi: 10.4161/worm.21833. PubMed
1213 PMID: 24058858; PubMed Central PMCID: PMCPMC3670459.
1214 57. Urmersbach B, Besseling J, Spies JP, Bringmann H. Automated analysis of sleep
1215 control via a single neuron active at sleep onset in C. elegans. Genesis. 2016;54(4):212-9.
1216 Epub 2016/02/03. doi: 10.1002/dvg.22924. PubMed PMID: 26833569.
1217 58. Bennett HL, Khoruzhik Y, Hayden D, Huang H, Sanders J, Walsh MB, et al.
1218 Normal sleep bouts are not essential for C. elegans survival and FoxO is important for
1219 compensatory changes in sleep. BMC neuroscience. 2018;19(1):10. Epub 2018/03/11.
1220 doi: 10.1186/s12868-018-0408-1. PubMed PMID: 29523076.
1221 59. White JG, Southgate E, Thomson JN, Brenner S. The structure of the nervous
1222 system of the nematode Caenorhabditis elegans. Philos Trans R Soc Lond B Biol Sci.
1223 1986;314(1165):1-340. Epub 1986/11/12. PubMed PMID: 22462104.
1224 60. Schafer WR, Kenyon CJ. A calcium-channel homologue required for adaptation
1225 to dopamine and serotonin in Caenorhabditis elegans. Nature. 1995;375(6526):73-8.
1226 Epub 1995/05/04. doi: 10.1038/375073a0. PubMed PMID: 7723846.
1227 61. Lee RY, Lobel L, Hengartner M, Horvitz HR, Avery L. Mutations in the alpha1
1228 subunit of an L-type voltage-activated Ca2+ channel cause myotonia in Caenorhabditis
1229 elegans. EMBO J. 1997;16(20):6066-76. Epub 1997/10/08. doi:
1230 10.1093/emboj/16.20.6066. PubMed PMID: 9321386.
1231 62. Mathews EA, Garcia E, Santi CM, Mullen GP, Thacker C, Moerman DG, et al.
1232 Critical residues of the Caenorhabditis elegans unc-2 voltage-gated calcium channel that
1233 affect behavioral and physiological properties. J Neurosci. 2003;23(16):6537-45. doi:
1234 10.1523/JNEUROSCI.23-16-06537.2003. PubMed PMID: 12878695; PubMed Central
1235 PMCID: PMCPMC6740628.

1236 63. Laine V, Frokjaer-Jensen C, Couchoux H, Jospin M. The alpha1 subunit EGL-19,
1237 the alpha2/delta subunit UNC-36, and the beta subunit CCB-1 underlie voltage-
1238 dependent calcium currents in Caenorhabditis elegans striated muscle. The Journal of
1239 biological chemistry. 2011;286(42):36180-7. Epub 2011/09/01. doi:
1240 10.1074/jbc.M111.256149. PubMed PMID: 21878625; PubMed Central PMCID:
1241 PMC3196126.
1242 64. Schuler C, Fischer E, Shaltiel L, Steuer Costa W, Gottschalk A. Arrhythmogenic
1243 effects of mutated L-type Ca 2+-channels on an optogenetically paced muscular pump in
1244 Caenorhabditis elegans. Sci Rep. 2015;5:14427. Epub 20150924. doi:
1245 10.1038/srep14427. PubMed PMID: 26399900; PubMed Central PMCID:
1246 PMCPMC4585839.
1247 65. Huang YC, Pirri JK, Rayes D, Gao S, Mulcahy B, Grant J, et al. Gain-of-function
1248 mutations in the UNC-2/CaV2alpha channel lead to excitation-dominant synaptic
1249 transmission in Caenorhabditis elegans. eLife. 2019;8. Epub 20190805. doi:
1250 10.7554/eLife.45905. PubMed PMID: 31364988; PubMed Central PMCID:
1251 PMCPMC6713474.
1252 66. Lin JY, Knutsen PM, Muller A, Kleinfeld D, Tsien RY. ReaChR: a red-shifted
1253 variant of channelrhodopsin enables deep transcranial optogenetic excitation. Nat
1254 Neurosci. 2013;16(10):1499-508. Epub 2013/09/03. doi: 10.1038/nn.3502. PubMed
1255 PMID: 23995068; PubMed Central PMCID: PMC3793847.
1256 67. Driver RJ, Lamb AL, Wyner AJ, Raizen DM. DAF-16/FOXO Regulates
1257 Homeostasis of Essential Sleep-like Behavior during Larval Transitions in C. elegans.
1258 Curr Biol. 2013;23(6):501-6. Epub 2013/03/13. doi: 10.1016/j.cub.2013.02.009. PubMed
1259 PMID: 23477722.
1260 68. Choi S, Chatzigeorgiou M, Taylor KP, Schafer WR, Kaplan JM. Analysis of
1261 NPR-1 reveals a circuit mechanism for behavioral quiescence in C. elegans. Neuron.
1262 2013;78(5):869-80. Epub 2013/06/15. doi: 10.1016/j.neuron.2013.04.002. PubMed
1263 PMID: 23764289; PubMed Central PMCID: PMC3683153.
1264 69. Spies J, Bringmann H. Automated detection and manipulation of sleep in C.
1265 elegans reveals depolarization of a sleep-active neuron during mechanical stimulation-
1266 induced sleep deprivation. Sci Rep. 2018;8(1):9732. Epub 2018/06/29. doi:
1267 10.1038/s41598-018-28095-5. PubMed PMID: 29950594.
1268 70. Stroustrup N, Ulmschneider BE, Nash ZM, Lopez-Moyado IF, Apfeld J, Fontana
1269 W. The Caenorhabditis elegans Lifespan Machine. Nat Methods. 2013;10(7):665-70.
1270 Epub 20130512. doi: 10.1038/nmeth.2475. PubMed PMID: 23666410; PubMed Central
1271 PMCID: PMCPMC3865717.
1272 71. Laurent P, Soltesz Z, Nelson GM, Chen C, Arellano-Carbajal F, Levy E, et al.
1273 Decoding a neural circuit controlling global animal state in C. elegans. eLife. 2015;4.
1274 Epub 20150311. doi: 10.7554/eLife.04241. PubMed PMID: 25760081; PubMed Central
1275 PMCID: PMCPMC4440410.
1276 72. Chun L, Gong J, Yuan F, Zhang B, Liu H, Zheng T, et al. Metabotropic GABA
1277 signalling modulates longevity in C. elegans. Nat Commun. 2015;6:8828. Epub
1278 20151105. doi: 10.1038/ncomms9828. PubMed PMID: 26537867; PubMed Central
1279 PMCID: PMCPMC4667614.
1280 73. Nagy S, Tramm N, Sanders J, Iwanir S, Shirley IA, Levine E, et al. Homeostasis
1281 in C. elegans sleep is characterized by two behaviorally and genetically distinct

1282 mechanisms. eLife. 2014;3:e04380. Epub 2014/12/05. doi: 10.7554/eLife.04380.
1283 PubMed PMID: 25474127; PubMed Central PMCID: PMC4273442.
1284 74. Alam MA, Kumar S, McGinty D, Alam MN, Szymusiak R. Neuronal activity in
1285 the preoptic hypothalamus during sleep deprivation and recovery sleep. J Neurophysiol.
1286 2014;111(2):287-99. Epub 2013/11/01. doi: 10.1152/jn.00504.2013. PubMed PMID:
1287 24174649; PubMed Central PMCID: PMC3921380.
1288 75. Brenner S. The genetics of Caenorhabditis elegans. Genetics. 1974;77(1):71-94.
1289 Epub 1974/05/01. PubMed PMID: 4366476.
1290 76. Stiernagle T. Maintenance of C. elegans. WormBook. 2006:1-11. Epub
1291 2007/12/01. doi: 10.1895/wormbook.1.101.1. PubMed PMID: 18050451.
1292 77. Ahringer A. Reverse genetics. WormBook, ed The C elegans Research
1293 Community. 2006. doi: doi/10.1895/wormbook.1.47.1.
1294 78. Redemann S, Schloissnig S, Ernst S, Pozniakowsky A, Ayloo S, Hyman AA, et
1295 al. Codon adaptation-based control of protein expression in C. elegans. Nat Methods.
1296 2011;8(3):250-2. Epub 2011/02/01. doi: nmeth.1565 [pii]10.1038/nmeth.1565. PubMed
1297 PMID: 21278743.
1298 79. Nagy S, Raizen DM, Biron D. Measurements of behavioral quiescence in
1299 Caenorhabditis elegans. Methods. 2014. Epub 2014/03/20. doi:
1300 10.1016/j.ymeth.2014.03.009. PubMed PMID: 24642199.
1301

1302

1303 **Figure Legends**

1304

1305 **Fig 1 – Strains expressing ion channel mutants in RIS**

1306 A) Scheme of the genetic design of the different RIS potassium channel mutant
1307 transgenes.

1308 B-D) Localization and expression of mKate2, which is translationally fused to the ion
1309 channels, in the different inactivation strains.

1310 E) Schematic representation of the genetic design of the RIS sodium channel mutant
1311 transgenes.

1312 F) Quantification of the expression levels of UNC-58gf::mKate2 in the two RIS
1313 overactivation strains. ***p<0.001, Welch test.

1314 G) Localization and expression of the strong overactivation strain (*RIS::unc-*
1315 *58gf(strong)*).

1316 H) Localization and expression of the weak overactivation strain (*RIS::unc-58gf(weak)*).

1317

1318 **Fig 2 – Survival of starvation-induced L1 arrest is a function of RIS activity**

1319 A) *RIS::twk-18gf* and *RIS::unc-58gf(strong)* strains cause divergent transcriptional
1320 profiles. Shown is the log2 fold change for all differentially expressed genes. A gene was
1321 counted as differentially expressed with an FDR<0.05. According to our previously
1322 published results, *RIS::twk-18gf* expressed 498 genes differentially compared with the
1323 wild type. *RIS::twk-18gf* has been shown to be similar to *aptf-1(gk794)* [24]. *RIS::unc-*
1324 *58gf(strong)* was shown to express 2913 genes differentially compared with the wild type
1325 [24]. Comparing *RIS::twk-18gf* and *RIS::unc-58gf(strong)* revealed 4676 differentially
1326 expressed genes. This analysis supports the view that these two strains have opposing
1327 transcriptional profiles and identifies 1910 additional genes that are potentially under the
1328 control of RIS activity (Table S5).

1329 B) Strong inactivation significantly decreases survival in L1 arrest whereas strong
1330 activation prolongs survival (three-parameter logistic fit, see also supplementary table S1,
1331 Fisher's Exact Test was conducted when 50% of wild-type worms were alive (day 22)).
1332 The p-values were FDR corrected with Benjamini-Hochberg procedure with a 5% false
1333 discovery rate. The plot includes data from three replicates. ***p<0.001.

1334 C) Recovery from L1 arrest depends on RIS activity with strong inactivation leading to a
1335 reduced recovery and constant activation leading to a prolonged ability to recover. For
1336 statistics, the Fisher's Exact Test was conducted at the time when 50% of wild-type
1337 worms recovered (day 23). The p-values were FDR corrected with Benjamini-Hochberg
1338 procedure with a 5% false discovery rate. The plot includes data from two replicates. N.s.
1339 $p>0.05$, *$p<0.05$, **$p<0.01$, ***$p<0.001$. Fisher's Exact Test.
1340
1341 **Fig 3 – Ion channel mutant expression in RIS controls baseline RIS activity**
1342 A) Ion channel expression in RIS results in a dose-response strain set with varying levels
1343 of RIS baseline activity. n.s. $p>0.05$, **$p<0.001$, ***$p<0.001$, Welch test with FDR
1344 correction for multiple testing.
1345 B) Long term RIS baseline activity for RIS activity strains from day 1 to day 12 of
1346 starvation.
1347
1348 **Fig 4 - Both, strong inactivation of RIS as well as *RIS::unc-58gf(strong)* prevent**
1349 **sleep behavior during L1 arrest**
1350
1351 A-F) Ion channel expression in RIS controls calcium activity and sleep behavior.
1352 Mobility quiescence bouts (grey shade) correlate with RIS transients. Movement speed
1353 was calculated by tracking the position of the head neuron RIS. A) *RIS::twk-18gf* and B)
1354 *RIS::egl-23gf(strong)* larvae do not have detectable mobility quiescence bouts or RIS
1355 transients. C) *RIS::egl-23gf(weak)* has reduced mobility quiescence bouts. D) Wild-type
1356 RIS activation transients and immobility bouts. E) *RIS::unc-58gf(weak)* spends more
1357 time in mobility quiescence bouts. F) *RIS::unc-58gf(strong)* has no detectable mobility
1358 quiescence bouts and no RIS transients but a high constant activity.
1359 G) RIS activation and immobility are correlated only for the strains that also show
1360 sleeping behavior. Alignment of RIS activity and speed to mobility quiescence bout
1361 onset. **$p<0.01$, ***$p<0.001$, Wilcoxon signed rank test.
1362 H) Mobility quiescence is a function of RIS activity levels n.s. $p>0.05$, **$p<0.001$,
1363 ***$p<0.001$, Welch test with FDR correction for multiple testing.
1364 I) Long-term sleep fraction for RIS activity strains from day 1 to day 12 of starvation.
1365

1366 **Fig 5 *RIS::unc-58gf* impairs sleep following cellular stress and during the L1 molt in**
1367 **developing larvae**
1368 A-F) Sleep fraction of worms of different RIS activity strains during the heat shock
1369 experiment. Animals were recorded continuously throughout the experiment. First, a 1h
1370 baseline was recorded at 22°C, then a 20min heat shock period of 37°C (in red shade) was
1371 applied, after the heat shock, the temperature was lowered to at 22°C again to monitor the
1372 response to the heat shock.
1373 G) Quantification of time spent in sleep 20 min after the heat shock. Wild-type worms
1374 sleep on average 38.3%. All other RIS manipulations reduced quiescence. *RIS::unc-*
1375 *58gf(strong)* only sleeps on average 6.5% of the time. **p<0.001, ***p<0.001, Welch test
1376 with FDR correction for multiple testing.
1377 H) *RIS::unc-58gf(strong)* reduces lethargus sleep compared to wild type. ***p<0.001,
1378 Welch test.
1379
1380 **Fig 6 – *RIS::unc-58gf(strong)* fails to inhibit wake-active circuits**
1381 A-B) Reduced global neuronal activity (grey shading) correlates with motion quiescence
1382 (supplementary movies S1-S6). Head speed was measured. A) sample trace, B) alignment
1383 of overall neuronal activity to mobility quiescence bout onset. ***p<0.001, Wilcoxon
1384 signed rank test.
1385 C) The mean neuronal inactivity fraction correlates with the mean mobility quiescence
1386 fraction (linear fit) for all strains.
1387 D) Strong RIS inactivation as well as *RIS::unc-58gf(strong)* caused an overall increase of
1388 neuronal activity. n.s. p > 0.05, *p<0.05, **p<0.01, ***p < 0.001, Welch test with FDR
1389 correction for multiple testing.
1390 E-F) RIM does not activate during mobility quiescence bouts. RIM speed was measured
1391 F) Sample trace (grey shade is RIM inactivity bout). Alignment of RIM activity and
1392 speed to mobility quiescence bout onset. *p<0.05, **p<0.01, ***p<0.001, Wilcoxon
1393 signed rank test.
1394 G) The mean RIM inactivity fraction correlates with the mean mobility quiescence
1395 fraction (linear fit) for all strains.

1396 H) Strong RIS inactivation as well as *RIS::unc-58gf(strong)* caused an overall increase of
1397 RIM activity. **p < 0.01, ***p < 0.001, Welch test with FDR correction for multiple
1398 testing.
1399
1400
1401 **Fig 7 – Phases of sensory PLM neuron inactivity occur during sleep and are strongly**
1402 **reduced in *RIS::unc-58gf(strong)* and *RIS::twk-18gf***
1403 A-C) Sample traces of PLM activity and speed in wild type, *RIS::unc-58gf(strong)* and
1404 *RIS::twk-18gf*. PLM speed was measured.
1405 D) *RIS::twk-18gf* and *RIS::unc-58gf(strong)* reduced phases of sensory neuron quiescence.
1406 *p<0.05, *** p<0.001, Welch test.
1407 E) *RIS::twk-18gf* and *RIS::unc-58gf(strong)* caused an overall increase of PLM activity.
1408 **p<0.01, ***p < 0.001, Welch test.
1409 F) *RIS::twk-18gf* causes increased PLM activity in detected quiescence as well as mobility
1410 bouts. *p<0.05, **p<0.01, ***p < 0.001, Welch test for comparison between strains,
1411 Wilcoxon signed rank test for comparison between the same strain quiescent and mobility
1412 bouts.
1413
1414 **Fig 8. *RIS::unc-58gf(strong)* causes increased muscle activity.**
1415 A) We calculated the movement speed of the RIM head neuron to measure head movement
1416 speed. RIM speed was reduced in *RIS::unc-58gf(strong)*. *p<0.05, **p<0.01, ***p <
1417 0.001, Welch test for comparison between strains, Wilcoxon signed rank test for
1418 comparison between the same strain quiescent and mobile bouts.
1419 B) We calculated the movement speed of the PLM tail neuron to measure tail movement
1420 speed. PLM movement speed was not significantly changed in mobile bouts in *RIS::unc-*
1421 *58gf(strong)* and increased in detected quiescent bouts. *p<0.05, **p<0.01, ***p < 0.001,
1422 Welch test for comparison between strains, Wilcoxon signed rank test for comparison
1423 between the same strain quiescent and mobile bouts.
1424 C-E) Sample traces of muscle activity for *RIS::twk-18gf* and *RIS::unc-58gf(strong)*.
1425 F) *RIS::unc-58gf(strong)* causes increased muscle activity in quiescence as well as mobility
1426 bouts. *p<0.05, **p<0.01, ***p < 0.001, Welch test for comparison between strains,

1427 Wilcoxon signed rank test for comparison between the same strain quiescent and mobility
1428 bouts.
1429 G) A sleep bout alignment reveals that *RIS::unc-58gf(strong)* has increased muscle
1430 activity. **p<0.01, ***p < 0.001, Wilcoxon signed rank test.
1431 H) *RIS::twk-18gf* and *RIS::unc-58gf(strong)* reduced phases of muscle inactivity.
1432 *p<0.05, Welch test.
1433
1434
1435 **Fig 9 *RIS::unc-58gf(strong)* is refractory to optogenetic activation of RIS**
1436 A) Optogenetic activation of RIS during the stimulation time (minute 1-2) leads to an
1437 increase of RIS activity and reduced mobility in wild-type worms but it does not affect
1438 the strong RIS activation strain. RIS speed was measured. A statistical comparison was
1439 made between baseline (0-1min) and stimulation (1-2min). n.s. p>0.05, **p<0.01,
1440 ***p<0.001, Wilcoxon signed rank test.
1441 B) Control for the optogenetic experiment. Without ATR treatment, neither the wild type
1442 nor the strong RIS activation strain, shows a response to green light. N.s. p>0.05,
1443 Wilcoxon signed rank test.
1444
1445
1446 **Fig 10 – Long-term optogenetic activation of RIS increases overall RIS calcium**
1447 **activity and promotes survival**
1448 A) Sample trace of control larvae without retinal in which RIS cannot be activated
1449 optogenetically. RIS speed was measured.
1450 B) Long-term optogenetic RIS activation by orange light in the presence of retinal.
1451 C) Long-term activation of RIS by ReaChR leads to an initial strong increase in calcium
1452 activity in RIS and simultaneous mobility quiescence followed by a mild RIS activity
1453 increase yet no increase in movement speed or movement quiescence.
1454 D) Comparison of RIS activity level changes caused by *RIS::unc-58gf(strong)* and by
1455 optogenetic activation of RIS. The data was normalized to their respective controls.
1456 E) Long-term optogenetic activation of RIS significantly increases RIS baseline. *p<0.05
1457 Welch test.

1458 F) Transients in RIS are significantly reduced in magnitude and don't correlate with
1459 quiescence. **p<0.01 Welch test.
1460 G) Long-term optogenetic activation of RIS inside microfluidic chambers leads to a small
1461 increase in survival (p=0.09 Logrank test, p=0.02 Fisher's Exact Test, the average of all
1462 individual worms of all three technical replicates was averaged, n=92 for
1463 *RIS::ReaChR*(+ATR), n=98 *RIS::ReaChR*(-ATR), n=124 wild type (+ATR), n=108 wild
1464 type (-ATR))
1465
1466
1467 **Fig 11 - RIS activates upon lethal blue-light stimulation and extends survival**
1468 A) Sample trace for a control worm stimulated by a short blue light stimulus. RIS speed
1469 was measured.
1470 B) Sample traces of wild-type worms upon stimulation with a long blue-light stimulus. The
1471 grey shaded area presents detected time in motion quiescence.
1472 C) The strong stimulus increased normalized RIS activity over baseline compared to
1473 control worms. ***p<0.001, Welch test.
1474 D) Wild-type worms have a survival advantage over RIS-inhibited worms upon exposure
1475 to the lethal blue-light stimulus. *p<0.05, Welch test.
1476
1477
1478 **Fig 12 – FLP-11 is required for sleep during L1 arrest**
1479 A) Deletion of the neuropeptide gene *flp-11* causes loss of sleep. Immobility in *RIS::unc-*
1480 *58gf(strong)* is increased when *flp-11* is deleted. ***p<0.001, Welch test with FDR
1481 correction for multiple testing.
1482 B) Loss of the FLP-11 neuropeptides leads to strongly reduced survival (three-parameter
1483 logistic fit, see also supplementary table S1, Fisher's Exact Test was conducted on day
1484 18) for comparisons when *flp-11(-)* was the shortest lived condition, day 20) when
1485 *RIS::unc-58gf(strong), flp-11(-)* was the shortest lived condition or day 24) when wild
1486 type was the shortest lived condition. The p-values were FDR corrected with Benjamini-
1487 Hochberg procedure with a 5% false discovery rate. The plot includes data from three
1488 replicates. ***p<0.001.
1489
1490

1491

1492 **List of Legends**

1493 The supplementary file includes:

1494 Supplementary text

1495 CRIPR sequences

1496 Supplementary Figures

1497 Fig S1 to S10

1498 Supplementary Tables

1499 Table S1 fitting parameters

1500 Table S2 strain list

1501 Table S3 primer list

1502 Table S4 p-values

1503 Table S5 DEG genes from the transcriptome data

1504 Movie legends for movies S1-S8

1505 References for the supplementary information

A

RIS manipulation	chromo-some	DNA sequence
RIS::egl-23gf(weak)	X	*flp-11p(endogenous)* | *flp-11b* | SL2 | *egl-23(L229N)* | linker | *mKate2* | *flp-11 3'UTR(endogenous)*
RIS::egl-23gf(strong)	X	*flp-11p(endogenous)* | *flp-11b* | SL2 | *egl-23(A383V)* | linker | *mKate2* | *flp-11 3'UTR(endogenous)*
RIS::twk-18gf	X	*flp-11p(endogenous)* | *flp-11b* | SL2 | *twk-18(e1913)* | linker | *mKate2* | *flp-11 3'UTR(endogenous)*

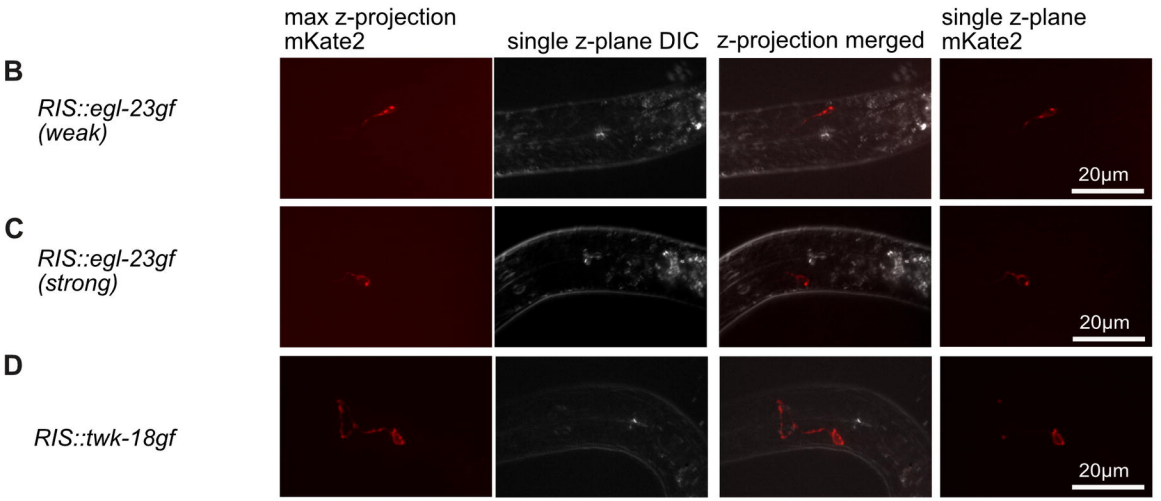

E

RIS manipulation	chromo-some	DNA sequence
RIS::unc58gf (strong)	X	*flp-11p(endogenous)* | *flp-11b* | SL2 | *unc-58(L428F)* | linker | *mKate2* | *flp-11 3'UTR(endogenous)*
RIS::unc58gf (weak)	III	*flp-11p(minimal)* | *unc-58(L428F)* | linker | *mKate2* | *flp-11 3'UTR(minimal)*

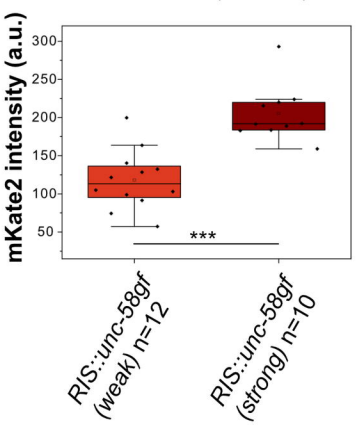

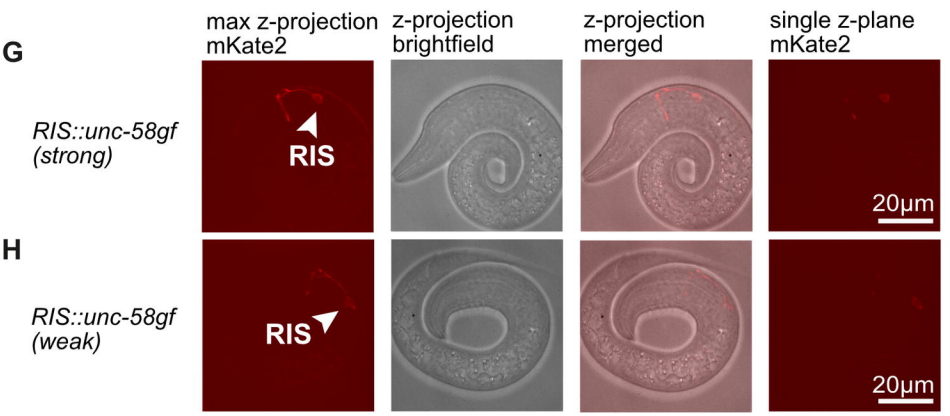

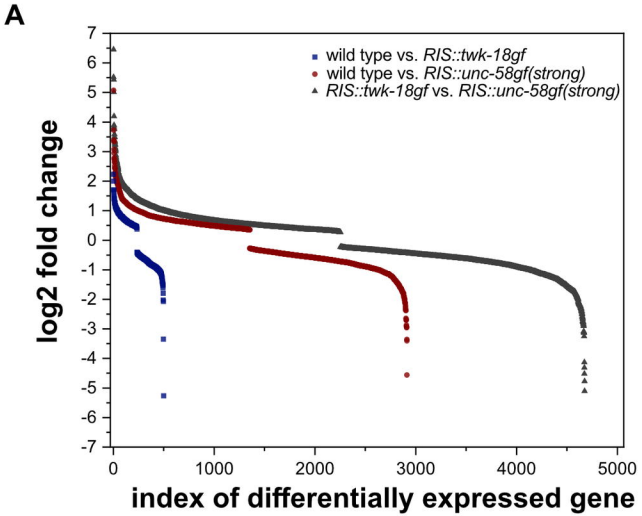
A
wild type vs. RIS::twk-18gf
wild type vs. RIS::unc-58gf(strong)
RIS::twk-18gf vs. RIS::unc-58gf(strong)
log2 fold change
index of differentially expressed gene

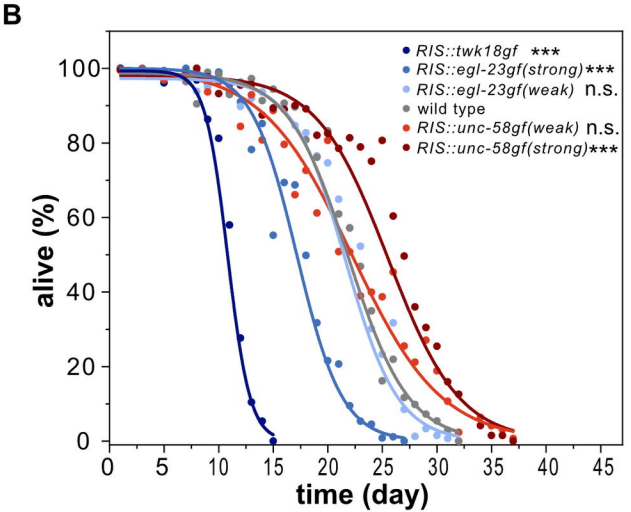
B
RIS::twk18gf ***
RIS::egl-23gf(strong)***
RIS::egl-23gf(weak) n.s.
wild type
RIS::unc-58gf(weak) n.s.
RIS::unc-58gf(strong)***
alive (%)
time (day)

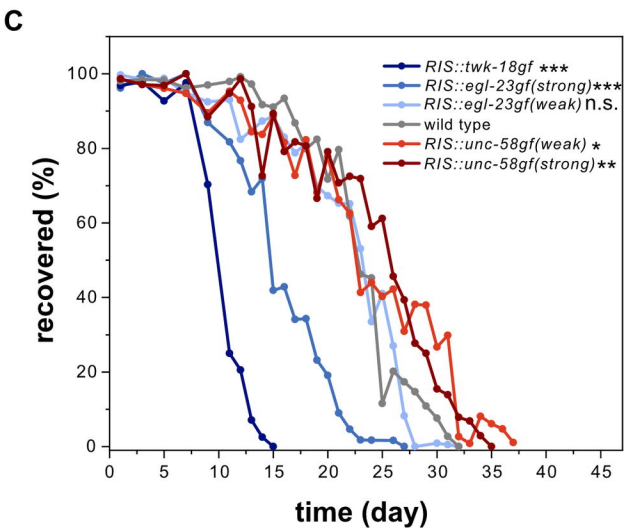
C
RIS::twk-18gf ***
RIS::egl-23gf(strong)***
RIS::egl-23gf(weak) n.s.
wild type
RIS::unc-58gf(weak) *
RIS::unc-58gf(strong)**
recovered (%)
time (day)

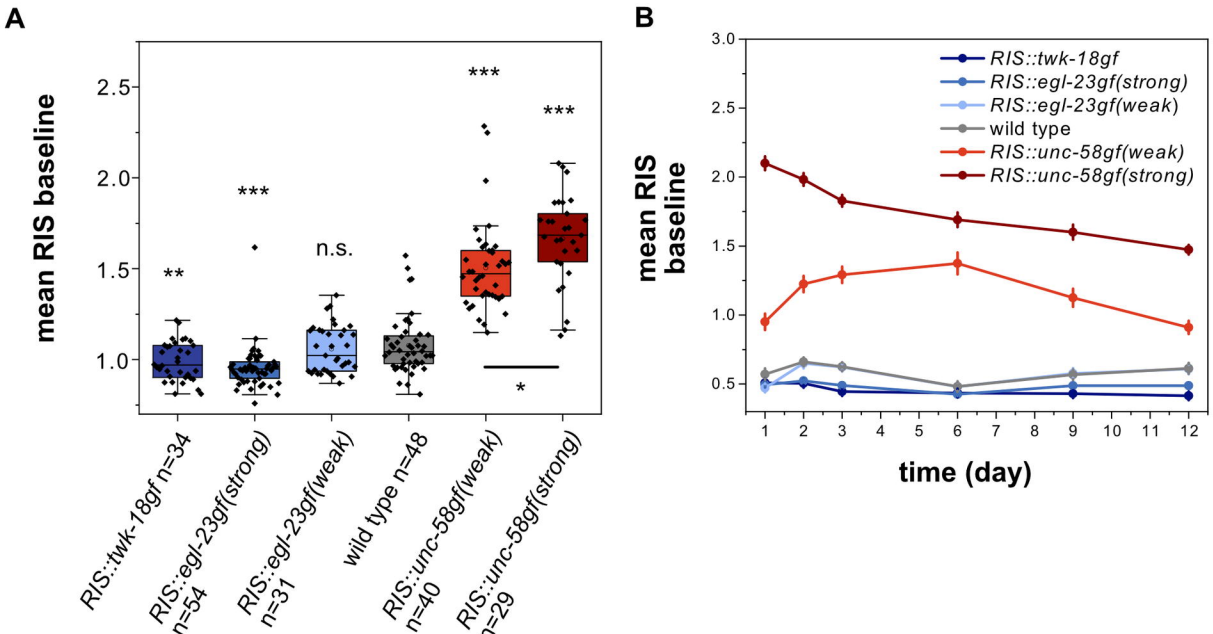
A
mean RIS baseline
2.5
2.0
1.5
1.0
**
***
n.s.
***
***
*
RIS::twk-18gf n=34
RIS::egl-23gf(strong) n=54
RIS::egl-23gf(weak) n=31
wild type n=48
RIS::unc-58gf(weak) n=40
RIS::unc-58gf(strong) n=29
B
mean RIS baseline
3.0
2.5
2.0
1.5
1.0
0.5
RIS::twk-18gf
RIS::egl-23gf(strong)
RIS::egl-23gf(weak)
wild type
RIS::unc-58gf(weak)
RIS::unc-58gf(strong)
1 2 3 4 5 6 7 8 9 10 11 12
time (day)

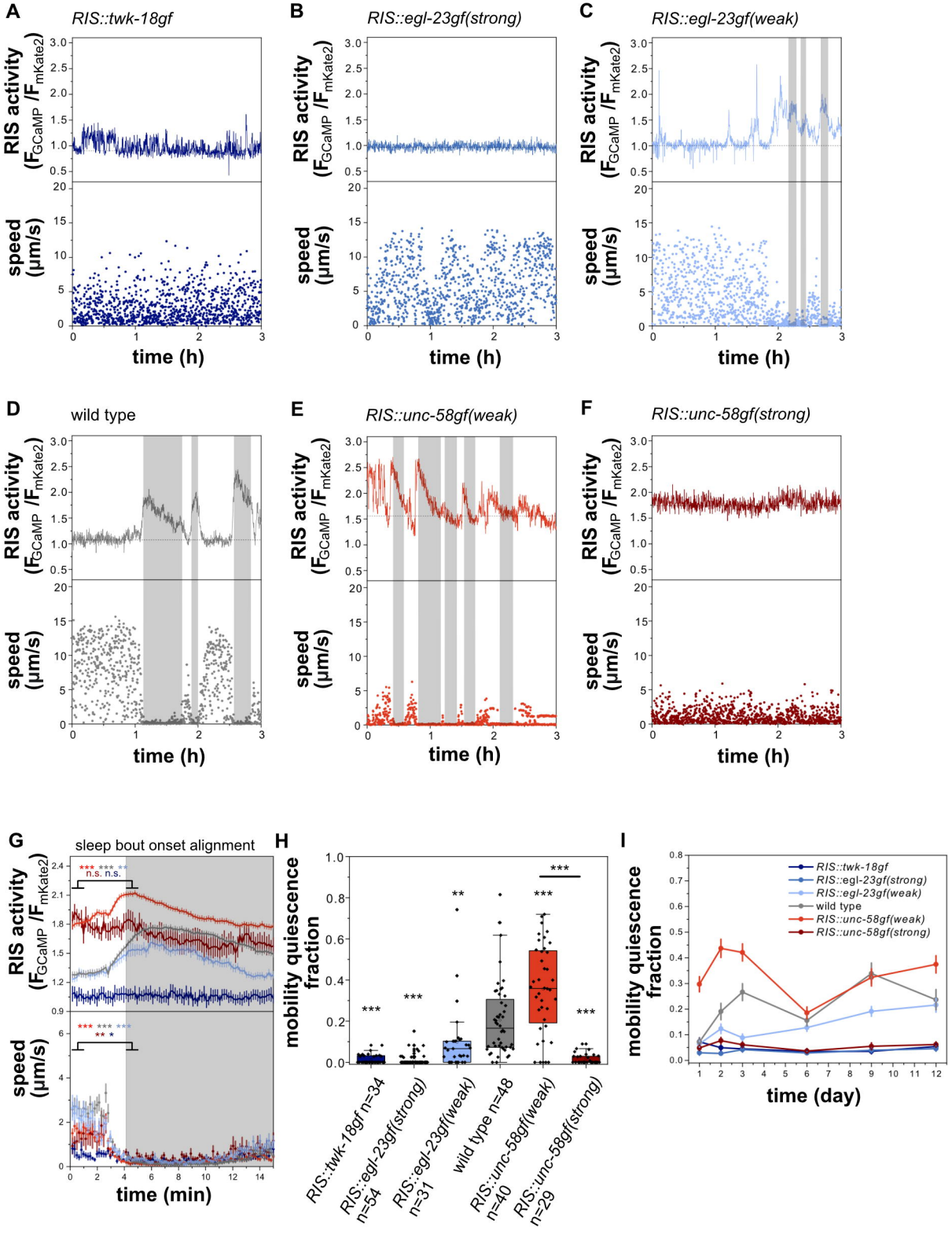
A
RIS::twk-18gf
B
RIS::egl-23gf(strong)
C
RIS::egl-23gf(weak)
D
wild type
E
RIS::unc-58gf(weak)
F
RIS::unc-58gf(strong)
RIS activity (F_{GCaMP} /F_{mKate2})
speed (µm/s)
time (h)
G
sleep bout onset alignment
n.s. n.s.
time (min)
H
mobility quiescence fraction
RIS::twk-18gf n=34
RIS::egl-23gf(strong) n=54
RIS::egl-23gf(weak) n=31
wild type n=48
RIS::unc-58gf(weak) n=40
RIS::unc-58gf(strong) n=29
I
RIS::twk-18gf
RIS::egl-23gf(strong)
RIS::egl-23gf(weak)
wild type
RIS::unc-58gf(weak)
RIS::unc-58gf(strong)
time (day)

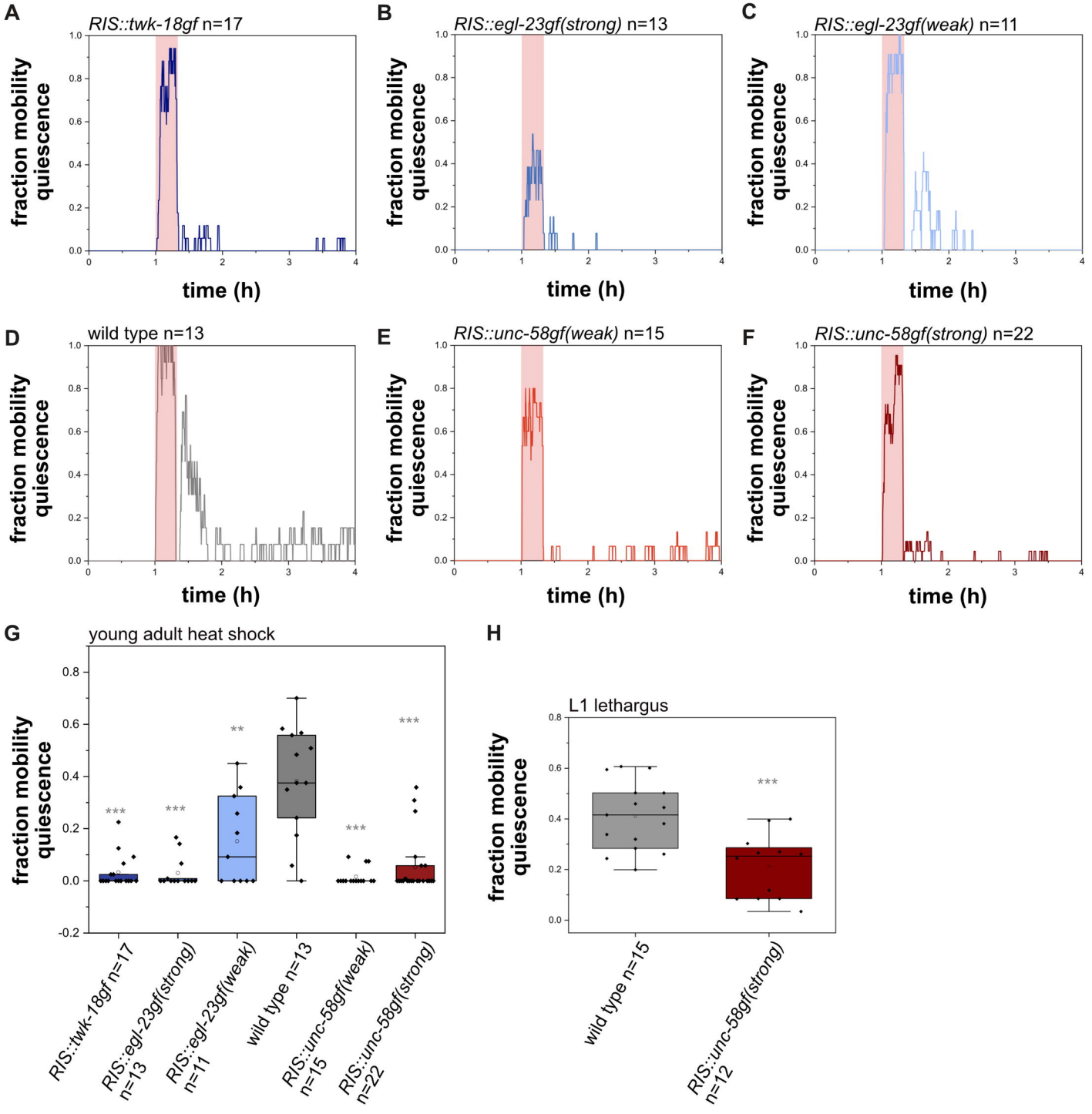
A
RIS::twk-18gf n=17
B
RIS::egl-23gf(strong) n=13
C
RIS::egl-23gf(weak) n=11
D
wild type n=13
E
RIS::unc-58gf(weak) n=15
F
RIS::unc-58gf(strong) n=22
fraction mobility quiescence
time (h)
G
young adult heat shock
fraction mobility quiescence
***
**
RIS::twk-18gf n=17
RIS::egl-23gf(strong) n=13
RIS::egl-23gf(weak) n=11
wild type n=13
RIS::unc-58gf(weak) n=15
RIS::unc-58gf(strong) n=22
H
L1 lethargus
fraction mobility quiescence
wild type n=15
RIS::unc-58gf(strong) n=12

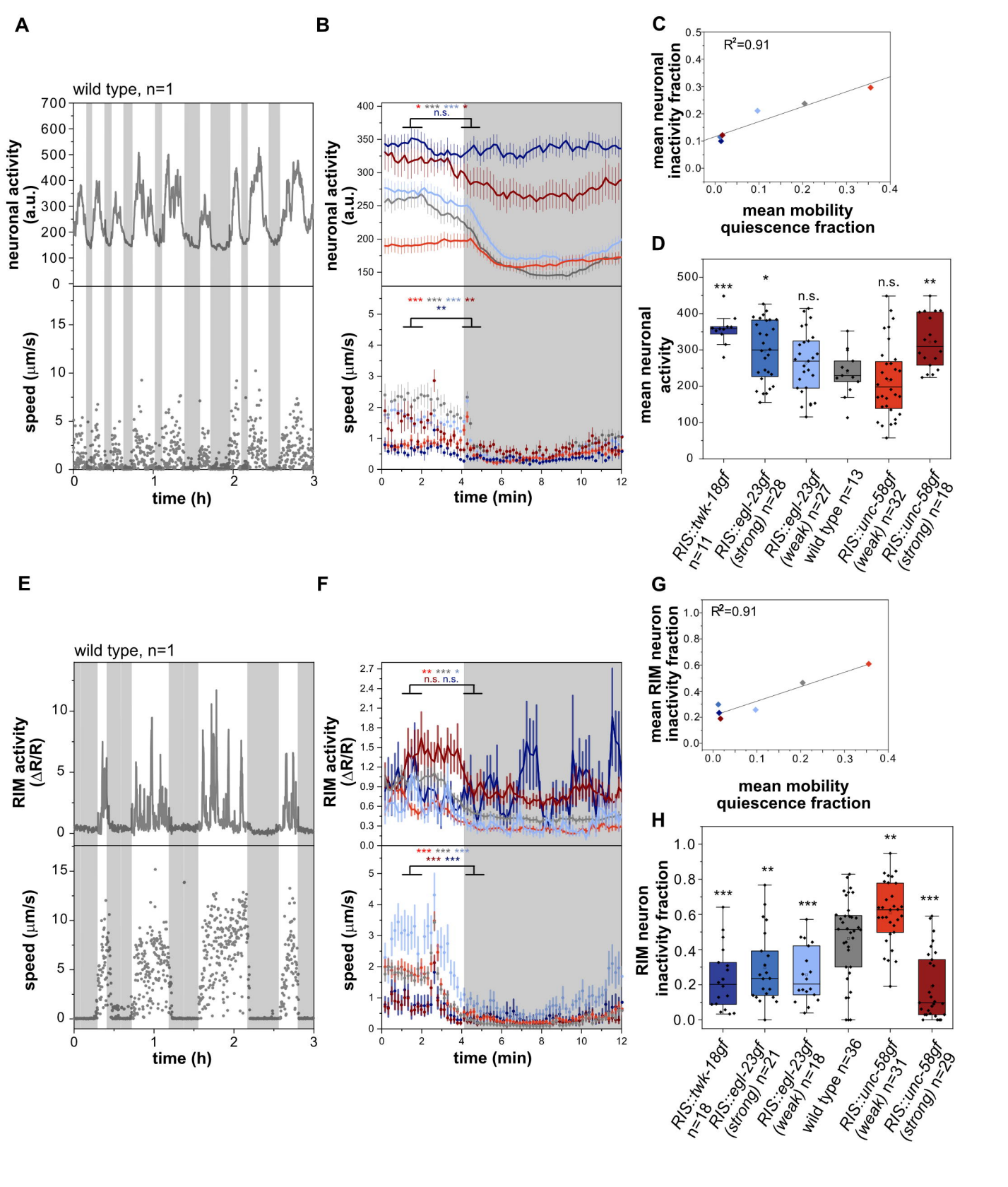
A
wild type, n=1
neuronal activity (a.u.)
speed (μm/s)
time (h)
B
n.s.
neuronal activity (a.u.)
speed (μm/s)
time (min)
C
R²=0.91
mean neuronal inactivity fraction
mean mobility quiescence fraction
D
mean neuronal activity
RIS::twk-18gf n=11
RIS::egl-23gf (strong) n=28
RIS::egl-23gf (weak) n=27
wild type n=13
RIS::unc-58gf (weak) n=32
RIS::unc-58gf (strong) n=18
E
wild type, n=1
RIM activity (ΔR/R)
speed (μm/s)
time (h)
F
n.s. n.s.
RIM activity (ΔR/R)
speed (μm/s)
time (min)
G
R²=0.91
mean RIM neuron inactivity fraction
mean mobility quiescence fraction
H
RIM neuron inactivity fraction
RIS::twk-18gf n=18
RIS::egl-23gf (strong) n=21
RIS::egl-23gf (weak) n=18
wild type n=36
RIS::unc-58gf (weak) n=31
RIS::unc-58gf (strong) n=29

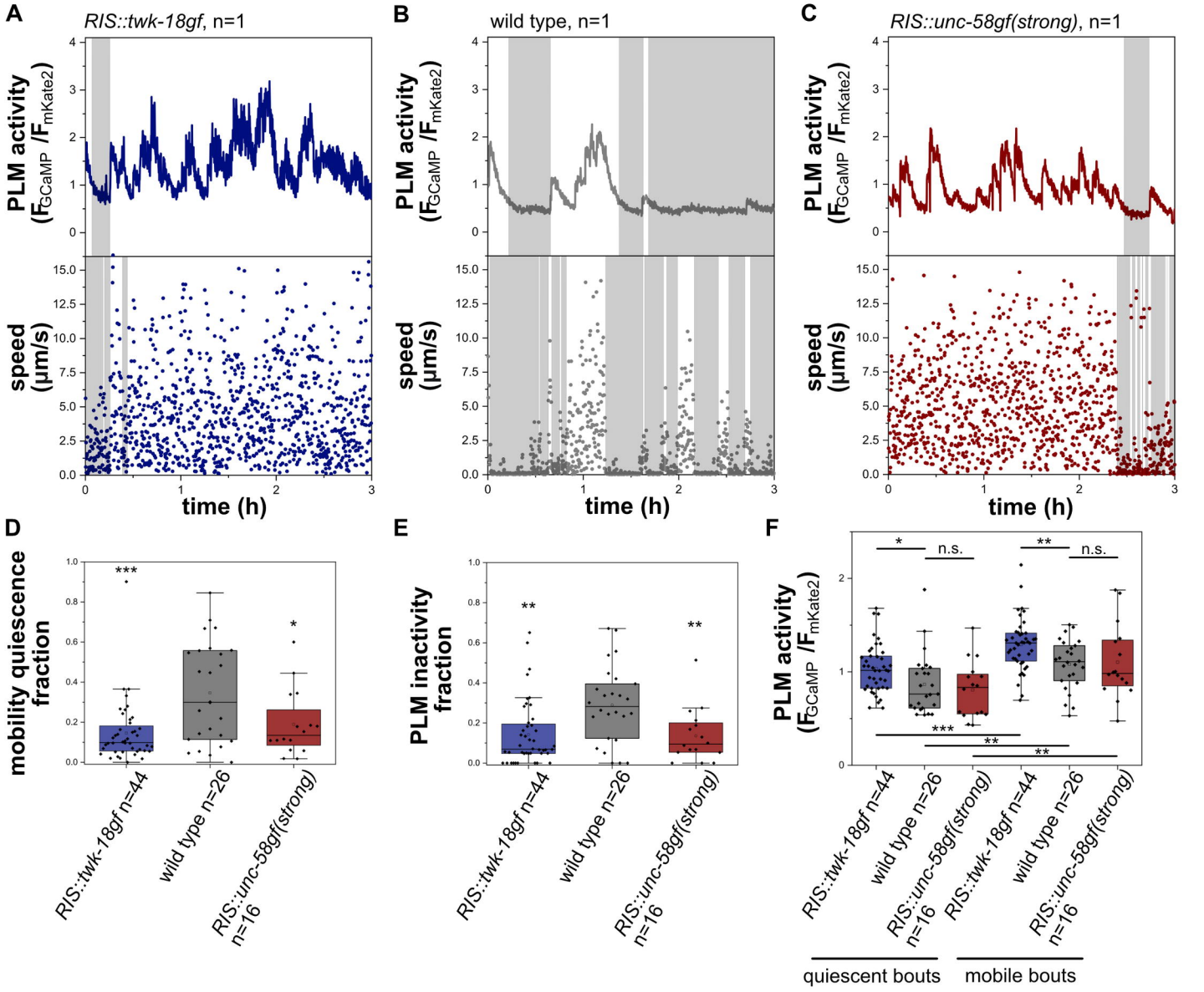
A
RIS::twk-18gf, n=1
B
wild type, n=1
C
RIS::unc-58gf(strong), n=1
PLM activity (FGCaMP /FmKate2)
speed (µm/s)
time (h)
D
mobility quiescence fraction
***
*
RIS::twk-18gf n=44
wild type n=26
RIS::unc-58gf(strong) n=16
E
PLM inactivity fraction
**
**
F
PLM activity (FGCaMP /FmKate2)
*
n.s.
**
n.s.
***
**
**
quiescent bouts
mobile bouts

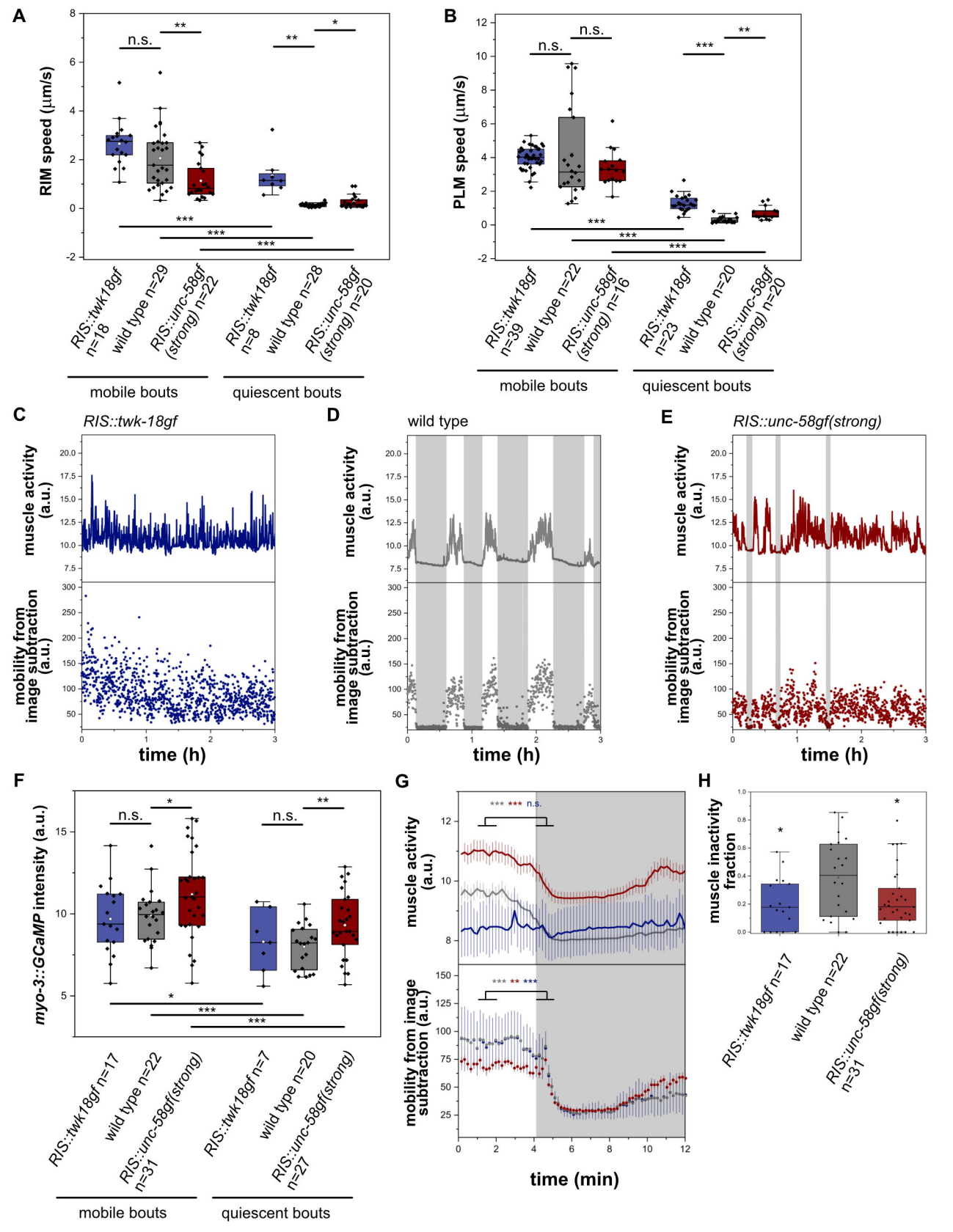
A
RIM speed (µm/s)
n.s.
**
**
*
***
***
***
RIS::twk18gf n=18
wild type n=29
RIS::unc-58gf (strong) n=22
RIS::twk18gf n=8
wild type n=28
RIS::unc-58gf (strong) n=20
mobile bouts
quiescent bouts
B
PLM speed (µm/s)
n.s.
n.s.
***
**
***
***
***
RIS::twk18gf n=39
wild type n=22
RIS::unc-58gf (strong) n=16
RIS::twk18gf n=23
wild type n=20
RIS::unc-58gf (strong) n=20
mobile bouts
quiescent bouts
C
RIS::twk-18gf
muscle activity (a.u.)
mobility from image subtraction (a.u.)
time (h)
D
wild type
muscle activity (a.u.)
mobility from image subtraction (a.u.)
time (h)
E
RIS::unc-58gf(strong)
muscle activity (a.u.)
mobility from image subtraction (a.u.)
time (h)
F
myo-3::GCaMP intensity (a.u.)
n.s.
*
n.s.
**
*
***
***
RIS::twk18gf n=17
wild type n=22
RIS::unc-58gf(strong) n=31
RIS::twk18gf n=7
wild type n=20
RIS::unc-58gf(strong) n=27
mobile bouts
quiescent bouts
G
*** *** n.s.
muscle activity (a.u.)
*** ** ***
mobility from image subtraction (a.u.)
time (min)
H
muscle inactivity fraction
*
*
RIS::twk18gf n=17
wild type n=22
RIS::unc-58gf(strong) n=31

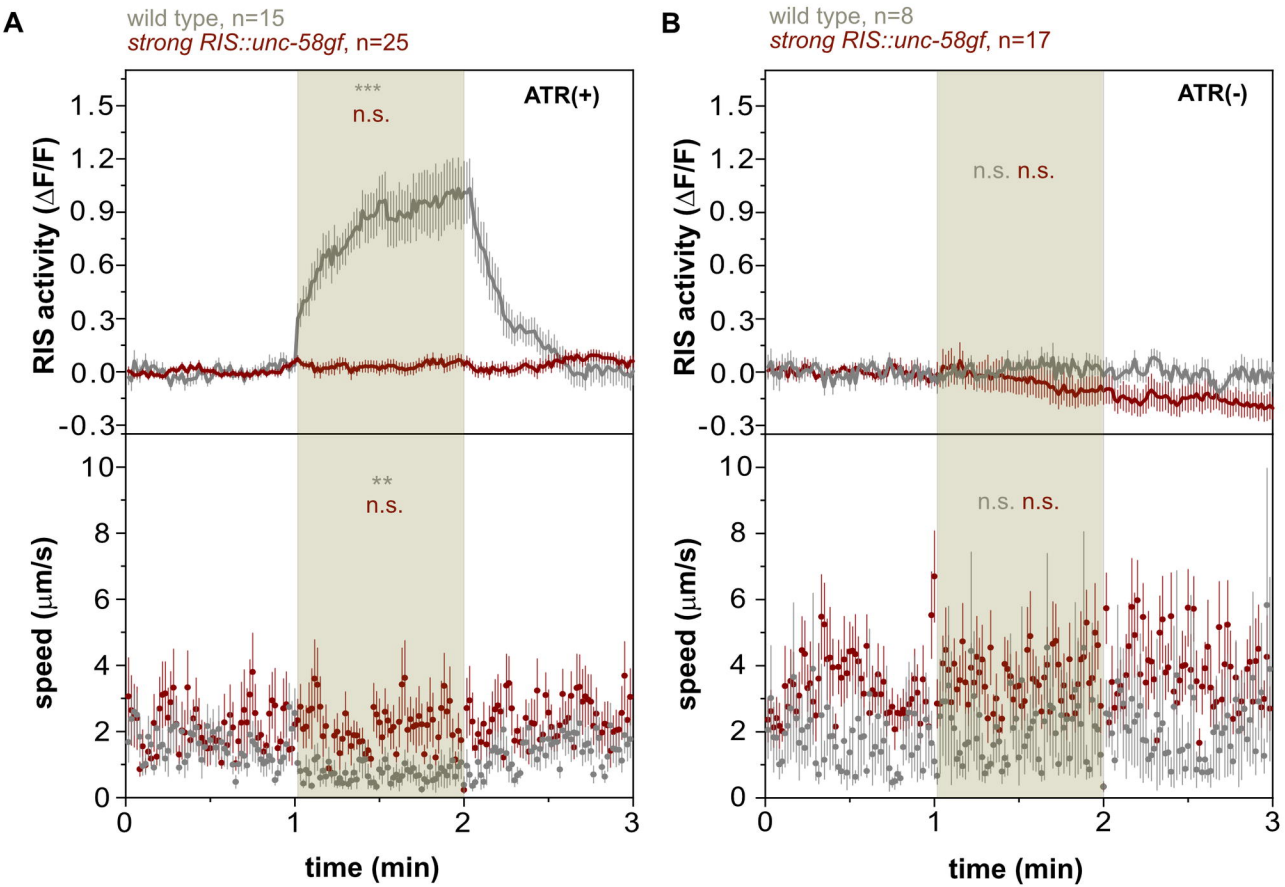
A
wild type, n=15
strong RIS::unc-58gf, n=25
ATR(+)
***
n.s.
**
n.s.
RIS activity (ΔF/F)
speed (μm/s)
time (min)
B
wild type, n=8
strong RIS::unc-58gf, n=17
ATR(-)
n.s. n.s.
n.s. n.s.
RIS activity (ΔF/F)
speed (μm/s)
time (min)

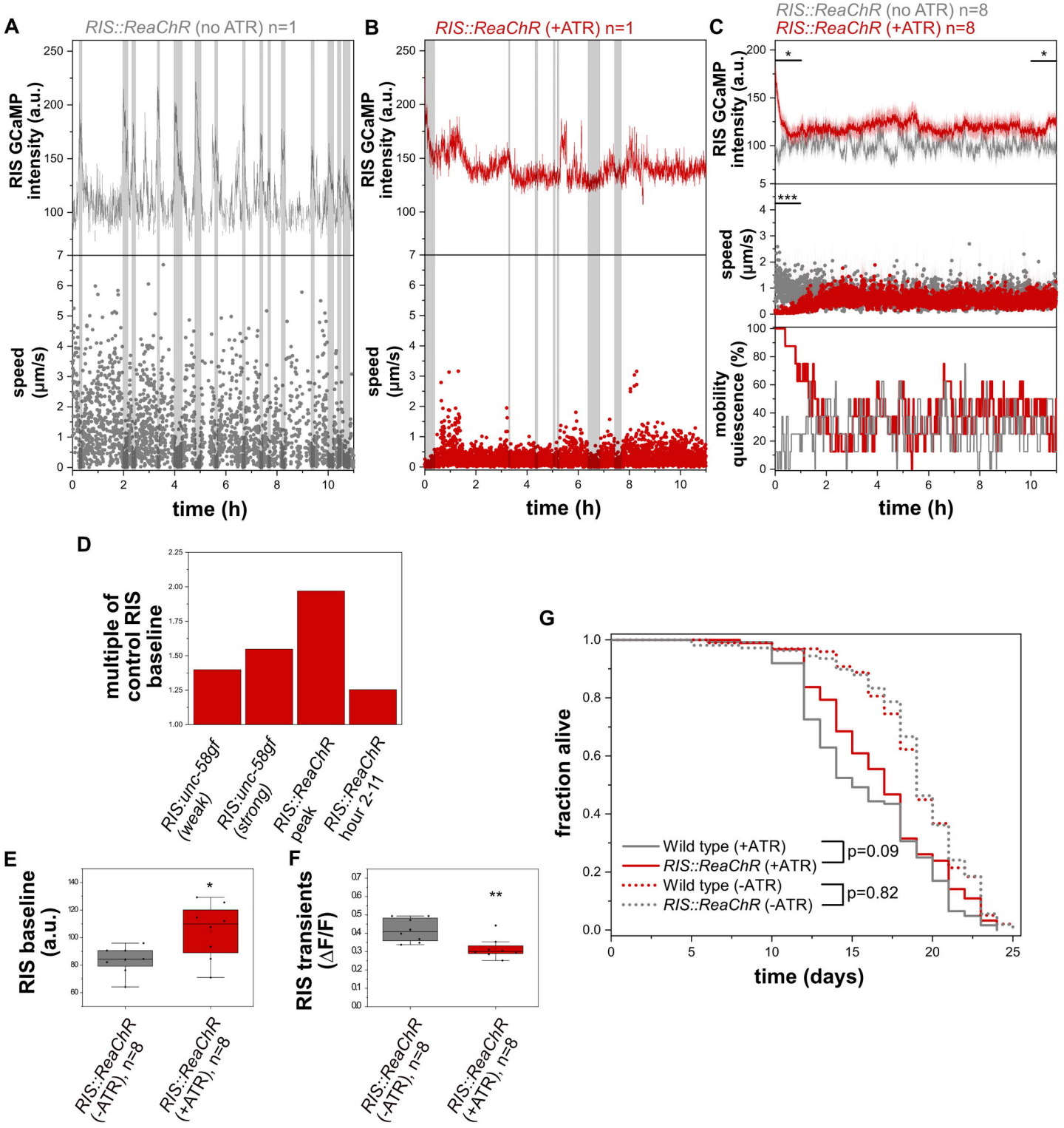
A
RIS::ReaChR (no ATR) n=1
RIS GCaMP intensity (a.u.)
speed (µm/s)
time (h)
B
RIS::ReaChR (+ATR) n=1
RIS GCaMP intensity (a.u.)
speed (µm/s)
time (h)
C
RIS::ReaChR (no ATR) n=8
RIS::ReaChR (+ATR) n=8
RIS GCaMP intensity (a.u.)
speed (µm/s)
mobility quiescence (%)
time (h)
D
multiple of control RIS baseline
RIS:unc-58gf (weak)
RIS:unc-58gf (strong)
RIS::ReaChR peak
RIS::ReaChR hour 2-11
E
RIS baseline (a.u.)
RIS::ReaChR (-ATR), n=8
RIS::ReaChR (+ATR), n=8
F
RIS transients (ΔF/F)
RIS::ReaChR (-ATR), n=8
RIS::ReaChR (+ATR), n=8
G
fraction alive
Wild type (+ATR)
RIS::ReaChR (+ATR)
Wild type (-ATR)
RIS::ReaChR (-ATR)
p=0.09
p=0.82
time (days)

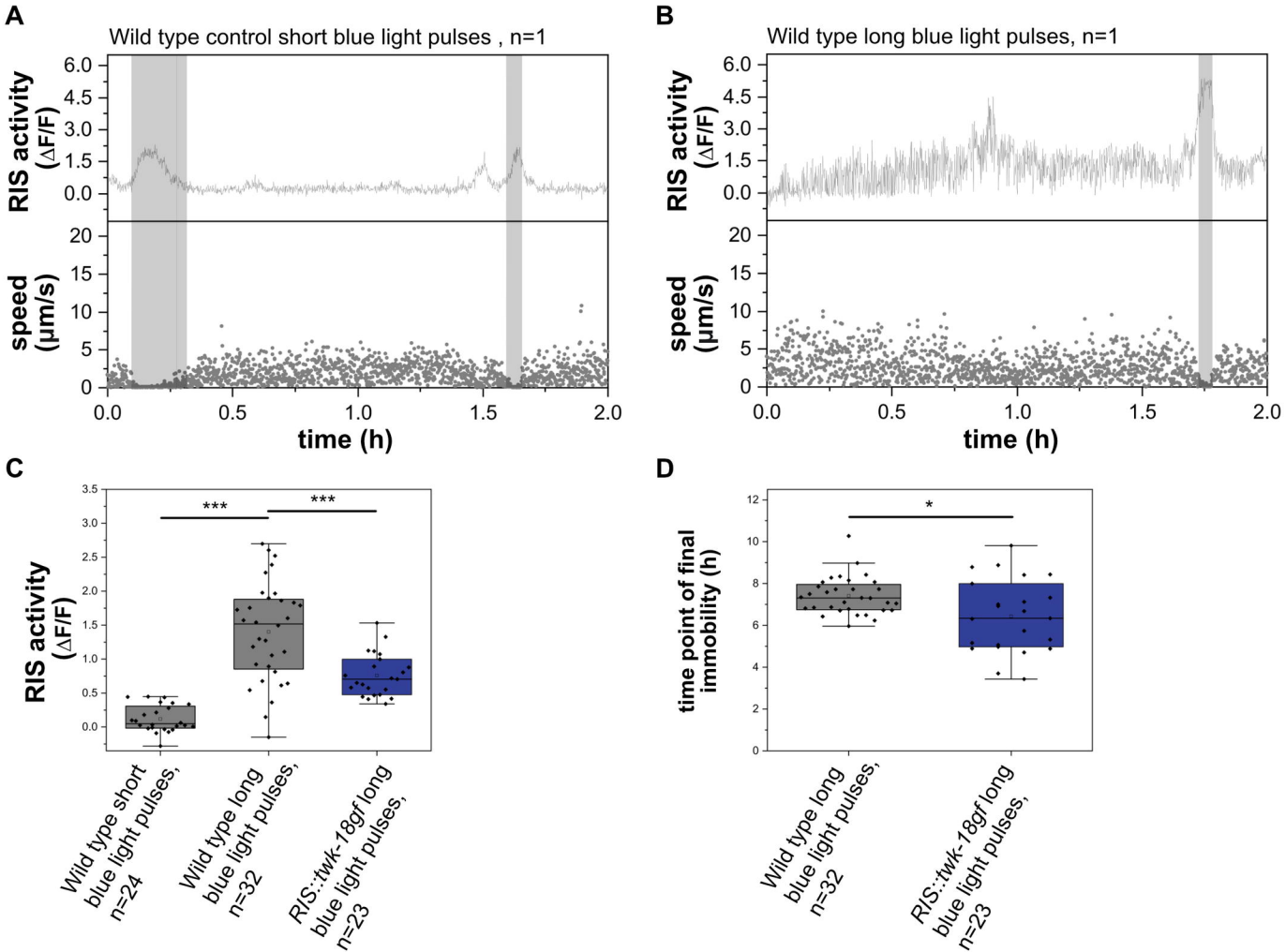
A
Wild type control short blue light pulses , n=1
RIS activity (ΔF/F)
speed (µm/s)
time (h)
B
Wild type long blue light pulses, n=1
RIS activity (ΔF/F)
speed (µm/s)
time (h)
C
RIS activity (ΔF/F)
***
***
Wild type short blue light pulses, n=24
Wild type long blue light pulses, n=32
RIS::twk-18gf long blue light pulses, n=23
D
time point of final immobility (h)
*
Wild type long blue light pulses, n=32
RIS::twk-18gf long blue light pulses, n=23

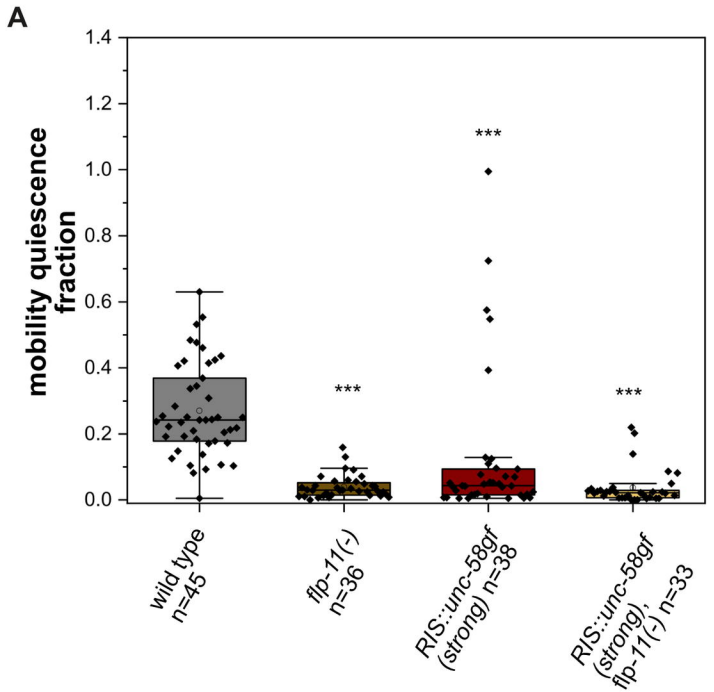
A
mobility quiescence fraction
1.4
1.2
1.0
0.8
0.6
0.4
0.2
0.0
***
***
***
wild type n=45
flp-11(-) n=36
RIS::unc-58gf (strong) n=38
RIS::unc-58gf (strong), flp-11(-) n=33

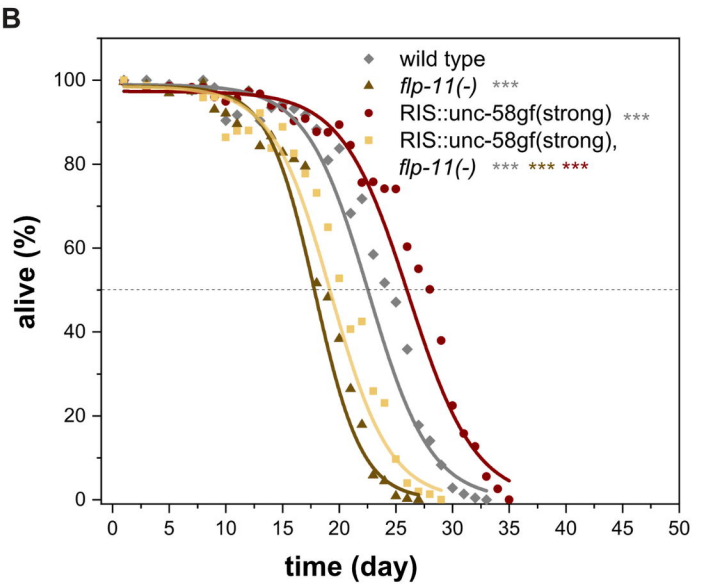
B
wild type
flp-11(-) ***
RIS::unc-58gf(strong) ***
RIS::unc-58gf(strong), flp-11(-) *** *** ***
alive (%)
100
80
60
40
20
0
0
5
10
15
20
25
30
35
40
45
50
time (day)